Critical Assessment of Common Force Fields for Molecular Dynamics Simulations of Potassium Channels

Critical assessment of common force fields for Molecular Dynamics simulations of potassium channels

Journal:	*Journal of Chemical Theory and Computation*
Manuscript ID	ct-2020-00331p.R2
Manuscript Type:	Article
Date Submitted by the Author:	n/a
Complete List of Authors:	Furini, Simone; Universita degli Studi di Siena, Department of Medical Surgery and Bioengineering Domene, Carmen; University of Bath, Chemistry

Critical assessment of common force fields for Molecular Dynamics simulations of potassium channels

Simone Furini[1,*] and Carmen Domene[2,3]

[1]Department of Medical Biotechnologies, University of Siena, Siena, Italy

[2]Department of Chemistry, University of Bath, Claverton Down, Bath BA2 7AY, United Kingdom

[3]Chemistry Research Laboratory, Mansfield Road, University of Oxford, Oxford OX1 3TA, United Kingdom

*Corresponding author:
Department of Medical Biotechnologies
University of Siena
Viale Mario Bracci, 16
53100 Siena, ITALY
Phone: +39 0577585297
Email: simone.furini@unisi.it

Abstract

For the last two decades, the KcsA K^+-channel has served as case-study to understand how potassium channels operate at the atomic scale, and Molecular Dynamics simulations have contributed significantly to the current knowledge of the atomic mechanisms of conduction, inactivation, and gating in this family of membrane proteins. Currently, microsecond trajectories are becoming the new standard in the field, and consequently, it is critical to assess and compare the performance of the classical force fields ordinarily used in simulations of biological systems, as well as quantitatively assess the agreement with experimental data for trajectories of this order of magnitude. To that extend, we performed classical Molecular Dynamics simulations with the CHARMM36 and AMBER-ff14sb force fields using atomic models based on the experimental structure of the KcsA channel in the open/conductive state, at conditions of ionic concentrations and membrane potentials resembling the ones adopted in experiments. In simulations using the CHARMM force field, the experimental open/conductive structure of the channel exhibited high conformational plasticity and a fast collapse towards an occluded state. In contrast, in an identical set of simulations using the AMBER force field, no major deviations from the experimental structure were recorded. Force field development is a complex process in which many approximations are typically required and adopted. The results presented here provide additional motivation to further improve the existing models, and crucially, alert practitioners about limitations.

Keywords

Ion channels; C-type inactivation; Conduction; Gating; Computational electrophysiology;

Introduction

The first quantitative description of ion currents across cell membranes dates back to the 1950's and to the pioneering work that culminated in the Hodgkin and Huxley model of action potential in excitable cells, which is still one of the greatest successes in the field of mathematical modelling of biological systems [1]. In the Hodgkin and Huxley model, Na^+ and K^+ membrane currents are described considering three functional properties: selectivity, gating, and inactivation. Currently, owing to the availability of high-resolution experimental structures of the proteins responsible for cell membrane currents – the ion channels – it is possible to investigate selectivity, gating, and inactivation at atomic scale using Molecular Dynamics (MD) simulations. MD simulations complement the knowledge gained from experimental structures providing dynamical information, and consequently, they have played a major role in ion channel research. In addition, the timescale accessible by MD simulations has rapidly increased in recent years, and consequently, some functional properties of ion channels, like the conductance, can now be estimated directly from MD trajectories. Under these circumstances, ion channels are once again at the frontiers in the field of mathematical modelling of biological systems, being one of the first and few cases where a direct link between atomistic simulations and macroscopic functional properties is possible. Likewise, we are in a unique position to test the accuracy of the simulation protocols and the energy functional forms, the force fields, traditionally used in MD simulations of biological systems. Force fields were originally developed in the eighties by direct comparison with experimental data or quantities obtained from relatively simple quantum calculations to current standards, and as more computational resources are becoming available, it has also become apparent that there is ample room for improvement.

The KcsA potassium channel is an ideal system to test how accurately MD simulations can reproduce the functional properties of ion channels. KcsA was the first K^+ selective ion channel to be resolved crystallographically in 1998 [2]. The pore of the channel is composed of four identical subunits, symmetrically arranged around the permeation axis. The selectivity filter, which is responsible for efficient and selective conduction of potassium ions, is in the P-loop region, at the extracellular entrance of the pore. This region includes five consecutive binding sites for potassium ions that are known as S0 to S4 starting from the extracellular side of the pore. At these binding sites, ions are coordinated by one (S0) or two rings (S1 to S4) of oxygen atoms contributed by residues $T_{75}V_{76}G_{77}Y_{78}G_{79}$ (Figure 1). It is well established that the ion current across KcsA is regulated by two mechanisms: opening/closing of the intracellular gate in response to changes in pH, and a decrease in the open probability of the channel over time at sustained pH values [3]. The inactivation process of KcsA is due to structural changes in the selectivity filter region, sharing many characteristics with C-type inactivation of eukaryotic channels [4]. In this respect, as the structure of

the selectivity filter is conserved among potassium channels, KcsA is considered a prototype for studying selective conduction and C-type inactivation in this family of membrane proteins [4–7].

Over the years, thanks to numerous MD simulation studies of KcsA and other K^+ channels, two alternative mechanisms for conduction of potassium ions have been proposed, considering or not water molecules involved in conduction events [8–15]. These two mechanisms will be referred as KWK and KK in what follows. The KWK mechanism was the first one to be proposed on the base of experimental data [16], free-energy perturbation calculations [8], and free-energy profiles estimated from atomistic simulations [11]. Subsequently, an alternative mechanism, denoted KK, was proposed, also on the basis of free-energy calculations [14]. Both conduction mechanisms share similar free energy landscapes, with local free-energy minima separated by low free-energy barriers. The main difference between these models of conduction resides in the presence or absence of vacancies or water molecules between ions in the selectivity filter, and whether or not ions bind at adjacent sites. The proposal of the KK mechanism from MD simulations led to reanalyse the electron densities from crystallographic experiments, which contrary to what was originally proposed on the basis of experimental data alone [16], confirmed the possibility that potassium ions occupy consecutive binding sites in the selectivity filter [15]. Despite conspicuous research efforts from both the computational and experimental communities, more than 20 years after the release of the first atomic structure of a K^+ channel, the microscopic features of conduction and selectivity are still a matter of intense debate [17 18]. In this scenario, MD simulation is a paramount method to investigate at atomic detail key features of conduction, selectivity, and gating, especially considering that simulations in the microsecond timescale are becoming routinely accessible. Crucially, results of MD simulations critically depend on the force field and simulation protocols adopted, and at present, quantitative agreement between microsecond trajectories and experimental observations needs to be verified.

In this study, MD simulations were performed using two atomic models of KcsA in the open/conductive state. One model, denoted KcsA-E71A, was based on the experimental structure of a KcsA mutant with glutamate at position 71 substituted by alanine [19]. The second model, denoted KcsA-WT, was identical to KcsA-E71A but with residue at position 71 modelled as glutamate, like in the wild-type channel. In the wild-type KcsA, opening of the lower gate causes the collapse of the selectivity filter, and this collapsed structure has been associated with the C-type inactivated state of the channel [5]. Experimental data and MD simulations have reported a H-bond between residues at positions 71 and 80 that assists the collapse of the selectivity filter [6]. As this H-bond is abolished in KcsA-E71A, inactivation is also compromised. Similarly, MD simulations also revealed an intricate network of H-bonds in the P-loop region, and an explanation for the role of water molecules at the back of the selectivity filter in the process of recovery from inactivation [7]. Nevertheless, an exhaustive

comparison of the degree of stability of the selectivity filter in simulations of wild-type KcsA and non-inactivating mutants using different force fields is still missing. This comparison could reveal novel insights into the inactivation process, and it will also asses the degree by which atomistic force fields are capable to capture and render information on the initial steps of this crucial process.

Here, MD simulations of KcsA-WT and KcsA-E71A models were performed under equilibrium conditions and with applied membrane potentials, using the AMBER-ff14sb and CHARMM36 force fields (referred as AMBER and CHARMM in what follows), two of the most widely-used force fields employed in simulations of membrane proteins, and more generally biological systems. KcsA-WT and KcsA-E71A trajectories revealed that the presence or absence of water molecules inside the selectivity filter has a major impact on its dynamics and its structure, with clear consequences on the inactivation process. The effects of the presence of water molecules on the structure of selectivity filter were found to be qualitatively similar in simulations using either AMBER or CHARMM force fields. In contrast, major differences between the two force fields emerged with respect to the stability of the open/conductive states of the channel in the microsecond timescale. As microsecond trajectories are rapidly becoming standard for the simulation of biological systems, the information that has emerged from this study should be critically considered by researchers working in the field.

Results

MD simulations including all possible combinations of the two channel models described (KcsA-WT and KcsA-E71A), using three membrane potentials (0 mV, +100 mV, and +200 mV), three force fields (AMBER, CHARMM, and CHARMM with NBFIX corrections for non-bonded interactions), and two initial loading states of the selectivity filter (KWK and KK) were considered. A detail summary of the simulated systems is presented in Table S1. At the start of the simulations, potassium ions were placed in positions S0, S2, and S4, while the remaining binding sites, S1 and S3, were vacant (in KK simulations) or occupied by water molecules (in KWK simulations). Four independent replicas were considered for each system unless otherwise stated. Most of the trajectories reached 1 μs, with the exception of some of the simulations where the selectivity filter collapsed on a shorter timescale (Table S1). More details about the simulation protocol are provided in the Methods section. Next, the results of MD simulations at equilibrium and with applied membrane potentials are described and compared for the trajectories obtained with the AMBER and the CHARMM/CHARMM-NBFIX force fields.

Equilibrium simulations using the AMBER force field

The stability of the open structure of the selectivity filter was assessed using its diameter, defined as the minimum distance between the G77 alpha carbon atoms in opposing subunits. This diameter is

respectively 8.1 Å and 5.5 Å in the experimental open and collapsed structures of the selectivity filter [20]. In simulations with the AMBER force-field, a diameter close to 8 Å was preserved, regardless of the channel model, KcsA-E71A or KcsA-WT, or the presence of water molecules in the initial loading state of the selectivity filter (Figure 1). However, significant dynamical differences emerged between trajectories with and without water molecules inside the selectivity filter. In simulations of KcsA-E71A starting from the KWK configuration, frequent exchanges of the ions in the selectivity filter between S2-S4 and S1-S3 sites were observed (Figure S1). In one out of the four trajectories, these transitions caused water molecules to leave the selectivity filter. Once water molecules left the selectivity filter, ions reorganized and occupied consecutive sites S2 and S3, remaining stable in such positions for the rest of the simulation (>800 ns). A similar behaviour was observed in all the trajectories of KcsA-E71A that started without water molecules inside the selectivity filter; i.e. ions rapidly moved to S2 and S3, and were stable in that configuration for most of the simulation time (Figure S1). The reduced mobility of ions in simulations lacking water molecules correlates with minor thermal fluctuations of the selectivity filter. The Root Mean Square Deviation (RMSD) of the backbone atoms of the selectivity filter of KcsA-E71A was 0.60±0.13 Å and 0.43±0.05 Å respectively in simulations with and without water molecules inside the selectivity filter (Figure 2). The higher RMSD in simulations with water molecules inside the selectivity filter is due to frequent flipping of the carbonyl oxygen atoms of V76 (Figure S2).

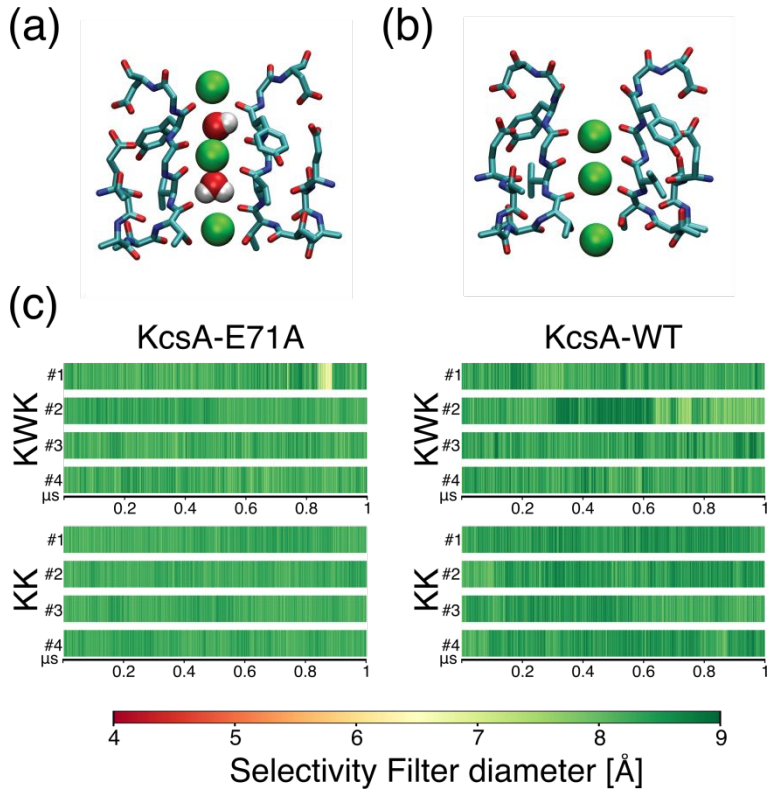

Figure 1. Distance between G77 alpha carbon atoms in opposing subunits in equilibrium simulations using the AMBER force field. (a-b) Representative snapshots of the selectivity filter in simulations of KcsA-WT, starting from the KWK and KK configuration respectively. Residues 71 to 80 are shown in licorice representation, ions and water molecules are shown as VDW spheres. Only two out of the four subunits are shown for simplicity. **(c)** Diameter of the selectivity filter in simulations of KcsA-E71A and KcsA-WT starting from KWK or KK configuration, using the AMBER force field. Four independent trajectories are shown for each combination of channel model and starting configuration of the selectivity filter. The colour maps indicate the minimum distance between G77 alpha carbon atoms in opposing subunits.

The equilibrium trajectories of KcsA-E71A presented earlier indicates that water molecules in binding sites S2 or S3 impact on the dynamics of the selectivity filter. Therefore, as structural changes of the selectivity filter are responsible for C-type inactivation, it is crucial to investigate the role of water molecules also in the KcsA-WT system, which in contrast to KcsA-E71A, is prone to inactivation. In the absence of water molecules, the behaviour of the selectivity filter is similar in KcsA-WT and KcsA-E71A. Binding sites S2 and S3 were occupied by ions with no intervening water molecules for most of the simulated time (Figure S3). Moreover, the presence of ions in S2 and S3 sites prevented flipping of V76 (Figure S2), reducing thermal fluctuations of the selectivity filter (Figure 2), as observed in the analogous simulations of KcsA-E71A. The only difference observed between KcsA-WT and KcsA-E71A simulations is a minor deviation in the psi backbone angle of Y78, which is caused by the H-bond established between Y78 and E71 in the wild-type channel (Figure S4). At odds with the high-similarity between simulations of KcsA-WT and KcsA-E71A starting from the KK configuration, the dynamics of the two models diverged in simulations starting from the KWK configuration. In the latter case, the RMSD of the backbone atoms of the selectivity filter (Figure 2) and the probability of V76 flipping (Figure S2) were higher in KcsA-WT than in KcsA-E71A (KcsA-WT RMSD is 0.70±0.11 Å versus 0.60±0.12 Å in Kcsa-E71A). On the basis of previous MD simulations, flipping of V76 was associated with a non-conductive state of the selectivity filter [21], and it was also proposed as a key step in the transition between the conductive and the C-type inactivated state [22]. In the simulations of KcsA-WT, the high-frequency of V76 flipping did not prevent ion translocations between S2-S4 and S1-S3 configurations. However, the translocation of ions did not facilitate the exit of water molecules from the selectivity filter in any of the simulations considered (Figure S3).

In summary, equilibrium simulations of KcsA-WT and KcsA-E71A with the AMBER force field revealed that the selectivity filter undergoes less thermal fluctuations when depleted of water

molecules, and that the effect of water molecules is more severe in the wild-type channel than in the non-inactivating mutant.

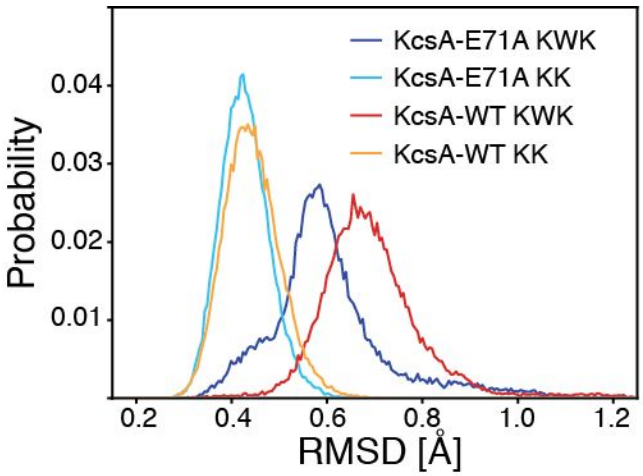

Figure 2. Root Mean Square Deviation of the selectivity filter backbone atoms in equilibrium simulations with the AMBER force field. The RMSD was measured for the backbone atoms of residues T75 to G79 with respect to the experimental conductive state of the selectivity filter (PDB entry 1K4C). The histograms were estimated using four independent trajectories starting respectively from the KWK/KK configurations of the selectivity filter for each of the simulated systems: KcsA-E71A starting from KWK (dark blue line), KcsA-E71A starting from KK (light blue line), KcsA-WT starting from KWK (red line), KcsA-WT starting from KK (orange line).

Simulations with applied membrane potentials using the AMBER force field

Departure of water molecules from the selectivity filter in equilibrium simulations of KcsA-E71A suggests a preference of the mutated channel for the KK over the KWK configuration. This preference was confirmed in simulations with constant electric fields acting in the direction of the channel axis, and mimicking the presence of membrane potentials. A set of simulations was performed starting with water molecules inside the selectivity filter and with membrane potential equal to +100 mV or +200 mV. The diameter of the selectivity filter was stable and close to ~8 Å, regardless of the channel model and membrane potential. In all the trajectories considered, the selectivity filter switched to a state with no water molecules in S2 and S3 in less than 300 ns (Figure S5). In addition, water molecules did not take part in any of the conduction events sampled during these trajectories (11 at +100 mV and 37 at +200 mV). Conduction events involved switching between two main configurations of the selectivity filter, with ions respectively in S2 and S3 or S0, S2, and S3, with a vacancy (nor water nor ion) in S1 (Figure 3). In simulations with membrane potential equal to +200 mV, ions were found at binding sites S2 and S3 with probability close to 100%, and the average occupancy of S0 was ~60%. In contrast, the S1 and S4 binding sites, were rarely occupied by ions

(Figure 3). The dynamics of the selectivity filter was similar to what was observed in equilibrium simulations in the absence of water molecules; RMSD values of the backbone atoms were 0.45±0.07 Å and flipping events of V76 were unlikely, confirming the stabilizing role exerted on the selectivity filter by the contemporary presence of ions in S2 and S3.

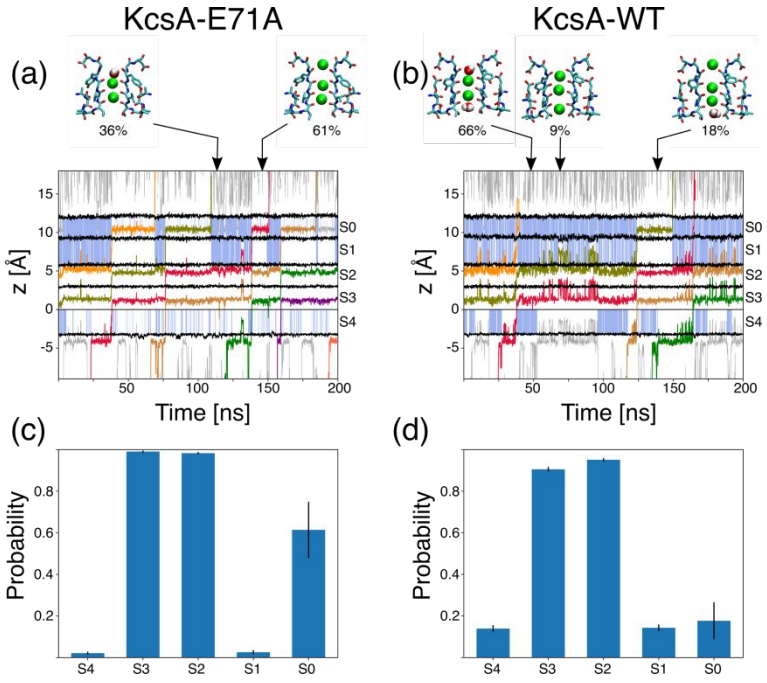

Figure 3. Ion conduction in simulations with membrane potential equal to +200 mV using the AMBER force field. (a-b) Ion positions along the axis of the channel are shown for a 200 ns interval of one replica (the entire trajectories are available as supplementary material), using thin grey lines for the ions outside the selectivity filter, and thick coloured lines for the ions inside the selectivity filter. All the coordinates are referred to the centre of mass of the carbonyl oxygen atoms of T75 residues (z = 0 Å). Thick black lines represent the centre of mass of the side chain oxygen atoms of T75, and the carbonyl oxygen atoms of V76, G77, Y79, and G79 from bottom to top. S0 to S4 labels indicate the positions of the ion binding sites. Binding sites are shaded in light blue when occupied by at least one water molecule. Snapshots of the selectivity filter are shown using licorice representation for residues 71-80, and VDW representation for ions and water molecules inside binding sites S1-S4. The probabilities of the different occupancy states of the selectivity filter were calculated using the entire simulation time of four independent replicas. Ions were considered at a binding site when their position along the permeation axis was in between the position of the centre of mass of each of the two rings of four oxygen atoms delimiting the corresponding binding site. **(c-d)** Percentage of ion occupancy for S0-S4 binding sites. Data collected from four independent trajectories are reported amounting to 4 μs for each channel model. Standard deviations among the four trajectories were calculated and are shown as vertical lines.

The rapid departure of water molecules from the selectivity filter observed in simulations of KcsA-E71A in the presence of membrane potentials did not take place in analogous simulations of KcsA-

WT. When the membrane potential was set to +100 mV, water molecules initially in S1 and S3 never left the selectivity filter, and no conduction event was sampled in any of the four independent trajectories considered, with a cumulative simulation time of 4 μs (Figure S6), whilst 11 conduction events were observed in the analogous set of simulations of KcsA-E71A. In simulations with membrane potential set to +200 mV, five conduction events were recorded (Figure S6) in contrast to 37 events in KcsA-E71A under the same conditions. A possible explanation for the lower conductance of KcsA-WT compared to KcsA-E71A is the fact that water molecules are more stable in the selectivity filter of the wild-type channel, and that consequently, it is harder to switch from the KWK to the KK configuration. In agreement with this hypothesis, switching from KWK to KK was observed in equilibrium simulations of KcsA-E71A, but not in equilibrium simulations of KcsA-WT. Moreover, four out of the five conduction events in simulations of KcsA-WT took place in the same trajectory that corresponds to the unique trajectory where water molecules were expelled from the selectivity filter. If the presence of water molecules is the actual barrier preventing ions from crossing KcsA-WT, the conductance should increase in simulations initialized with ions and not water molecules inside the selectivity filter. This hypothesis was confirmed in simulations of KcsA-WT starting from the KK configuration. When water molecules were not present in the selectivity filter, the number of conduction events recorded was 4 at +100 mV and 34 at +200 mV (Figures S7); these results resemble the data obtained for the KcsA-E71A system (respectively 11 and 37). The lower conductivity of KcsA-WT compared to KcsA-E71A might easily be explained by minor differences in the dynamics of the selectivity filter. Compared to KcsA-E71A, the probability of observing ions in S0, S2 and S3 decreased (18% in KcsA-WT versus 61% in KcsA-E71A), while the probability of observing ions only in S2 and S3 increased (66% in KcsA-WT versus 36% in KcsA-E71A), and a state with ions in S1, S2 and S4 emerged with probability ~9% (the probability of this state was lower than 1% in KcsA-E71A). As a consequence, whilst binding sites S2 and S3 are occupied with high probability in both channel models, the average occupancy of S0 is much lower in the wild-type model than in the mutant (Figure 3). Negligible occupancy of S0 is likely correlated to the presence of an H-bond between residues Y78 and E71 that structurally modifies the lower boundary of S0 in KcsA-WT compared to KcsA-E71A.

The estimated conductance at +200 mV was 7.4±0.8 pS and 6.8±4.3 pS for KcsA-E71A and KcsA-WT respectively (standard deviation computed among replicas). Noticeably, when the intracellular gate is locked in the open state, like in the atomic structures used in this study, the experimental conductance with symmetrical ion concentrations of 200 mM is around 200 pS, which is one order of magnitude higher than the estimated value [19].

Equilibrium simulations using the CHARMM force field

The same set of simulations presented previously using the AMBER force field were also performed with the CHARMM force field and are discussed next. The first remarkable difference between the two sets of simulations is the facility of the selectivity to collapse when the CHARMM force field is used, an event that was never observed in the simulations with the AMBER force field (compare Figure 1 with Figure 4). In MD trajectories, the selectivity filter was considered to have switched to a collapsed state when its diameter averaged over the last 10 ns of the trajectory was lower than 5.5 Å. In none of the simulated trajectories, the selectivity filter recovered to the canonical open configuration after such a collapsing event. In simulations of KcsA-E71A, collapse events were observed in three out of four trajectories when the initial state of the selectivity filter included water molecules, and in two out of four trajectories when water was not present in the selectivity filter at first. When the analysis is restricted to the trajectories where the selectivity filter collapses, the time of the collapsing event is respectively 347±282 ns and 617±77 ns in sets with/without water molecules initially inside the selectivity filter. The times of the collapsing events were estimated as averages and standard deviations among independent trajectories. Due to the limited number of trajectories, these values should be considered only as approximations. However, the shorter time interval for the first collapsing event observed in simulations starting from the KWK configuration compared to simulations starting from the KK configuration seems to support the hypothesis that the presence of water molecules inside the selectivity filter destabilize the open/conductive state. In order to better characterize the dynamics of the selectivity filter, the trajectories of KcsA-E71A with collapsing events were synchronized using as reference the time of the collapse as defined above. This analysis revealed that collapsing is associated with an increase in the number of water molecules behind the selectivity filter (Figure 5), in agreement with previous MD simulations [22]. As a reference, the number of water molecules in the same region in simulations with the AMBER force field is stable at 9 ± 1 (standard deviation computed among replicas). The deviation of the selectivity filter from the experimental open/conductive structure and the increase in the number of water molecules behind the selectivity filter appears as concurrent events, and so it was not possible to establish a causal link between the entrance of water molecules and the collapsing of the selectivity filter. Instead, the two processes seem to reinforce each other, until a critical threshold is reached, and the selectivity filter switches to a collapsed state (Figure 5). A similar behaviour was observed in simulations of KcsA-WT, where in all instances, the selectivity filter switched to a collapsed state, regardless of the presence or absence of water molecules inside the selectivity filter. The time when the first collapsing event occurs was slightly quicker in simulations starting with water molecules inside the selectivity filter, 346±201 ns, compared to simulations starting from a water-free selectivity filter, 460±248 ns,

which once again supports the hypothesis that water molecules destabilize the open/conductive structure of the selectivity filter. Analogous dynamics of the selectivity filter were observed in simulations using the CHARMM force field including correction terms for non-bonded interactions (NBFIX), with rapid collapsing of the selectivity filter both in simulations of KcsA-WT and KcsA-E71A, in the presence or absence of water molecules (Figure S8). On average, collapse of the selectivity filter was faster in simulations with NBFIX terms than in simulations using the standard CHARMM parameters for ions. Another set of simulations was performed using the ion parameters developed by Joung and Cheatham [23], like in the AMBER simulations described in previous sections, in combination with the CHARMM force field for protein and lipids. The behaviour of the selectivity filter in these trajectories was comparable to the other CHARMM trajectories, with large deviations from the experimental conductive structure of the selectivity filter (Figure S9).

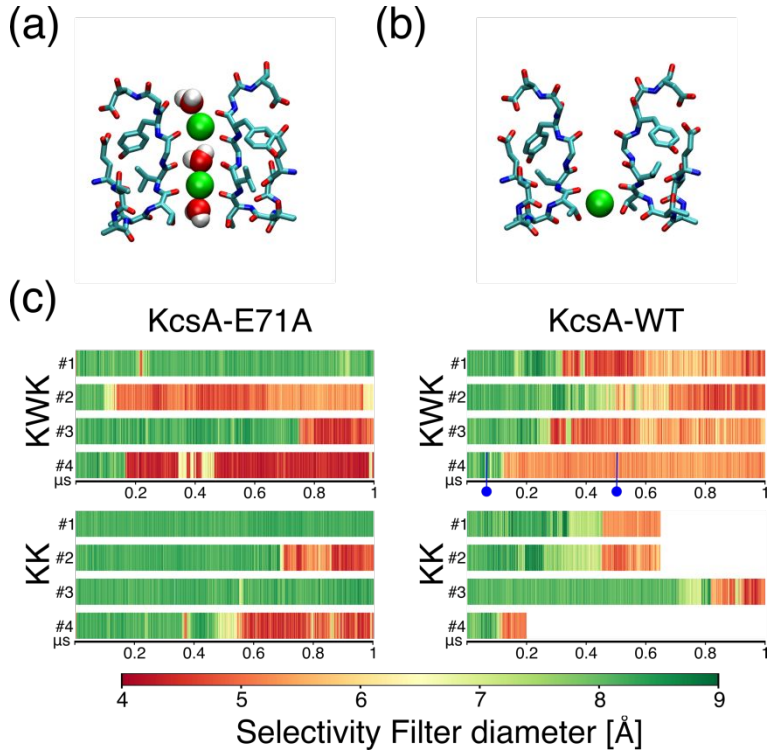

Figure 4. Distance between G77 alpha carbon atoms in opposing subunits in equilibrium simulations using the CHARMM force field. (a-b) Snapshot of the selectivity filter in simulations of KcsA-WT before and after a collapsing event. Snapshots were taken from replica #4 of KcsA-WT starting with a KWK loading state, as indicated by the blue markers in the corresponding colour map. Residues 71 to 80 are shown in licorice representation, ions and water molecules are shown as VDW spheres. **(c)** Diameter of the selectivity filter in simulations of KcsA-E71A and KcsA-WT starting from KWK or KK configurations. Four independent trajectories are shown for each combination of channel model and starting configuration of the selectivity filter. The colour maps reflect the minimum value of the distance between G77 alpha carbon atoms in opposing subunits.

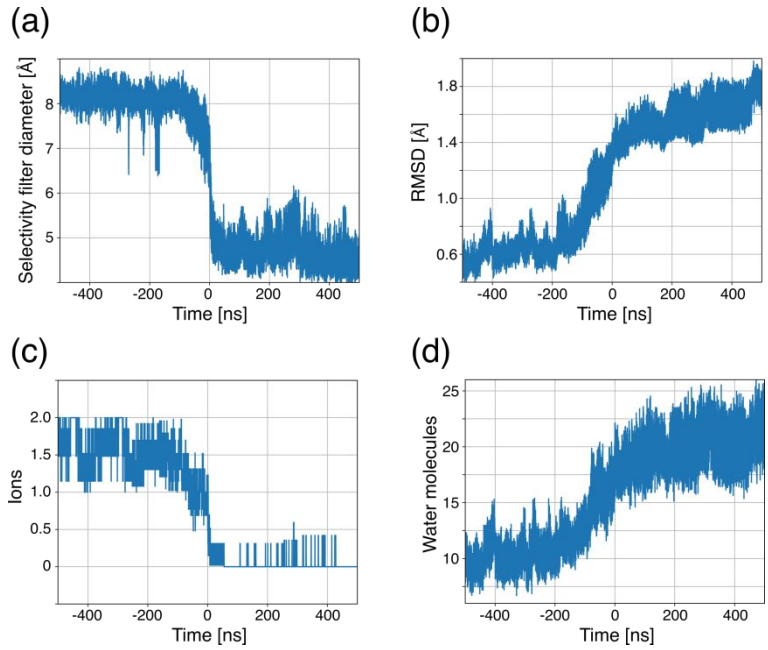

Figure 5. Collapse events of the selectivity filter in equilibrium simulations of KcsA-E71A with the CHARMM force field. The trajectories where the selectivity filter collapses (replicas 2,3,4 in simulations starting from the KWK loading state; replicas 2 and 4 in simulations starting from the KK loading state) were synchronized using the time of such event (t = 0 ns in the plots). The average and the standard errors calculated over independent replicas are shown for: (a) minimal distance between G77 alpha carbon atoms in opposing subunits; (b) RMSD of the backbone atoms of residues T75 to G79 with respect to the experimental open structure of the selectivity filter (PDB entry 1K4C); (c) number of ions in binding sites S3, S2 and S1; (d) water molecules within 6 Å from carbonyl oxygen atoms of residues T75, V76 and G77.

Simulations with applied membrane potentials using the CHARMM force field

The collapsing of the selectivity filter observed in equilibrium simulations of KcsA-WT and KcsA-E71A is obviously correlated with the distribution of ions inside the channel, as the selectivity filter cannot collapse if binding site S2 is occupied by an ion. Thus, since the presence of a membrane potential affects ion dynamics, it is also likely to affect the break-down of the open structure of the selectivity filter. Indeed, in simulations of KcsA-E71A, conformational changes of the selectivity filter were observed only in one out of four trajectories when the membrane potential was equal to +100 mV, and in none of the four trajectories with membrane potential equal to +200 mV (Figure 6). All the trajectories of KcsA-E71A in the presence of membrane potentials were initialized with water molecules inside the selectivity filter. However, with the exception of a single conduction event at +100 mV, all the other conduction events did not involve water molecules (Figure 7 and Figure S10). While the preference for the KK mechanism is a common feature in simulations with AMBER and CHARMM force fields, the fine details of conduction events are different. In simulations using AMBER, binding sites S2 and S3 were mostly occupied by ions, and conduction events consisted of

an incoming ion entering S3 and pushing the ions already inside the selectivity filter from S3 and S2 toward S2 and S0. This same conduction mechanism was observed also in simulations using CHARMM. However, the state with ions in S2 and S3, and not in S0, was less likely is simulations using CHARMM (10%) than in simulations using AMBER (36%). Moreover, in CHARMM simulations, KcsA-E71A also exhibited an alternative conduction route; where ions bind to S1, S2, and S4, (S3 empty) and conduction is initiated by an incoming ion pushing the ions first towards S0, S2, and S3, and finally re-establishing the S1, S2, and S4 configuration with the exit of the outermost ion towards the extracellular space. This alternative conduction route represents ~20% of the total number of conduction events sampled in the four replicas. As a consequence of the different conduction strategies, the distribution of ions inside the selectivity filter is also different, with the CHARMM force field exhibiting higher occupancy of S1 and lower occupancy of S3 with respect to the AMBER force field (compare Figure 3 with Figure 7). Not surprisingly, this difference with regard to conduction mechanisms between the two force fields is also reflected on the estimated conductance values, which are higher for CHARMM (19.0±3.8 pS at +200 mV) compared to AMBER (7.4±0.8 pS at +200 mV) force field.

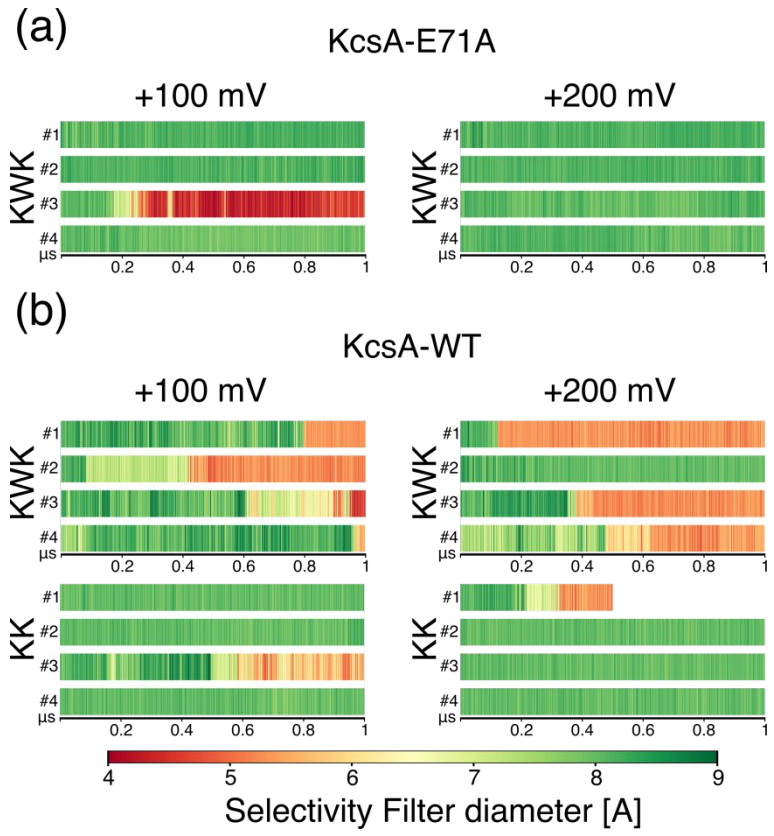

Figure 6. Distance between G77 alpha carbon atoms in opposing subunits in equilibrium simulations using the CHARMM force field. Diameter of the selectivity filter in simulations of (a) KcsA-E71A, and (b) KcsA-WT starting from KWK or KK configurations. Four independent

trajectories are shown for each set. The colour maps reflect the minimum value of the distance between G77 alpha carbon atoms in opposing subunits.

In the equilibrium MD simulations presented in the previous section, the selectivity filter of KcsA-WT was more prone to collapse than the selectivity filter of KcsA-E71A. Since the presence of an electric field in the direction of the channel axis impacts on the stability of the selectivity filter in KcsA-E71A, it is essential to evaluate its effect on the wild-type, inactivating channel, as well. Indeed, striking differences emerged between simulations of KcsA-E71A and KcsA-WT in the presence of membrane potentials equal to +100 mV and +200 mV. When water molecules were included in the selectivity filter at the beginning of the simulation, KcsA-WT collapsed in all the four trajectories with membrane potential equal to +100 mV, and in three out of the four trajectories with membrane potential equal to +200 mV, compared to a single collapsing trajectory for KcsA-E71A (Figure 6). The selectivity filter collapsed at 547±257 ns compared to 346±201 ns in equilibrium simulations, which suggests that the electric field has a stabilizing effect on the open structure, as it was also observed for KcsA-E71A. However, at odds with the non-inactivating channel, in KcsA-WT the stabilizing effect of the electric field is not sufficient to prevent the break-down of the open structure of the selectivity filter. Moreover, in the single trajectory where the selectivity filter did not collapse, not a single conduction event was observed in 1 μs despite the membrane potential was equal to +200 mV (Figure S11). Simulations using the CHARMM force field with NBFIX corrections exhibited a rapid collapse of the selectivity filter in all the trajectories, regardless of the channel model and membrane potential (Figures S12), and consequently, this combination was not investigated further.

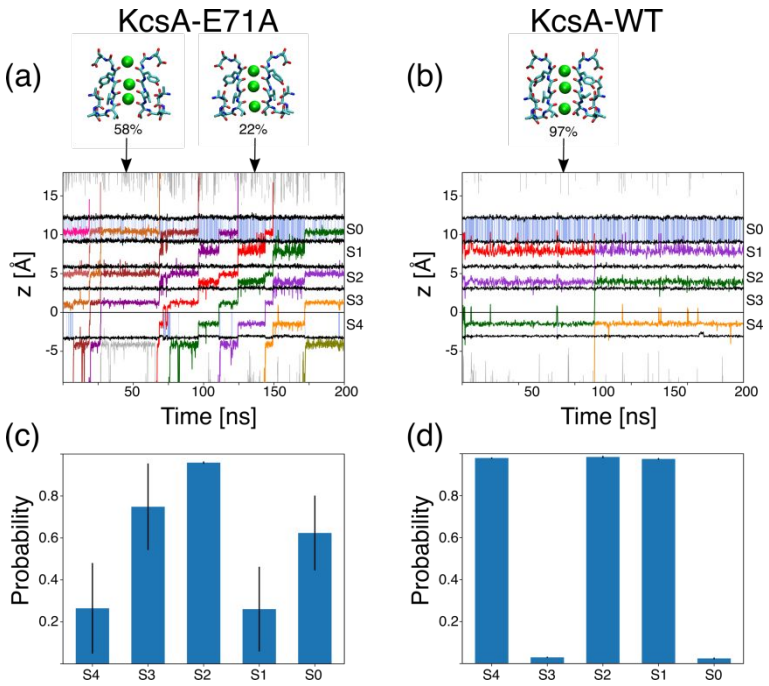

Figure 7. Ion conduction in simulations with membrane potential equal to +200 mV using the CHARMM force field. (a-b) Ion positions along the axis of the channel are shown for a 200 ns interval of one replica (the entire trajectories are available as supplementary material), using thin grey lines for the ions outside the selectivity filter, and thick coloured lines for the ions inside the selectivity filter. All the coordinates are referred to the centre of mass of the carbonyl oxygen atoms of T75 residues (z = 0 Å). Thick black lines corresponds to the centre of mass of the side chain oxygen atoms of T75, and the carbonyl oxygen atoms of V76, G77, Y79, and G79 from bottom to top. S0 to S4 labels indicate the positions of the ion binding sites. Binding sites are shaded in light blue when occupied by at least one water molecule. Representative snapshots of the selectivity filter are shown using a licorice representation for residues 71-80, and ions and water molecules inside binding sites S1-S4 are shown in van der Waals representation. The probabilities of the different occupancy states of the selectivity filter were calculated using the cumulative simulation time of four independent replicas. Ions were considered at a binding site when their position along the permeation axis was in between the position of the centre of mass of each of the two rings of four oxygen atoms delimiting the corresponding binding site. **(c-d)** Percentage of ion occupancy for S0-S4 binding sites. Data collected from four independent trajectories are reported amounting to 4 μs for each channel. Standard deviations of the four trajectories were calculated and are shown as vertical lines.

As the presence of water molecules promotes destabilization of the selectivity filter, simulations of KcsA-WT in the presence of membrane potentials and starting without water molecules inside the selectivity filter were considered next. In agreement with equilibrium simulations, the absence of water molecules decreased the propensity of the selectivity filter to collapse. Both with membrane potential equal to +100 mV and +200 mV, the break-down of the open structure was observed only in one out the four trajectories (Figures 6). More surprisingly, the fact that the structure of the selectivity filter remained stable did not correlate with an increase in the number of conduction events across the channel (Figures S13). In trajectories where the selectivity filter was stable in the open

configuration, one conduction event was observed at +100 mV (over 3 μs) and two conduction events were observed at +200 mV (over 3 μs), compared to 15 (over 3 μs) and 95 (over 4 μs) in KcsA-E71A. For most of the simulated time, ions occupy binding sites S1, S2, and S4, a configuration that was observed also in simulations of KcsA-E71A but that seems particularly stable for KcsA-WT (Figure 7). The different behaviour observed at the lower boundary of S0 is probably prompted by the ability of the protein to establish a H-bond between residues Y78 and E71 which prevent ions from changing easily between (S1, S3, S4) and (S0, S2, S3) configurations. Another feature that characterized the simulations of KcsA-WT with applied membrane potentials was the presence of extremely low thermal fluctuations. The RMSD value of the backbone atoms of the selectivity filter was 0.34±0.05 Å, a value remarkably lower than the one observed in analogous simulations with the AMBER force field (Figure 2) or in simulations of KcsA-E71A with the CHARMM force field (Figure 8).

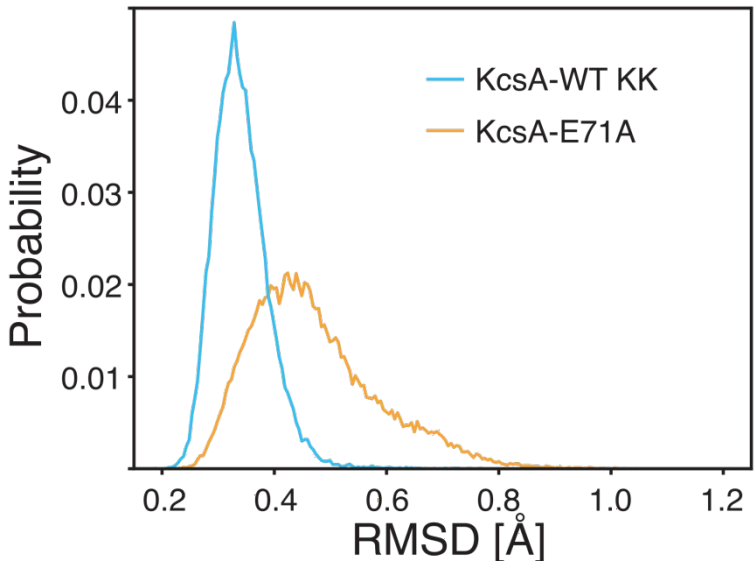

Figure 8. Root Mean Square Deviation of the selectivity filter backbone atoms in simulations with the CHARMM force field. The RMSD was measured for the backbone atoms of residues T75 to G79 with respect to the experimental conductive state of the selectivity filter (PDB entry 1K4C). The histograms were estimated using four trajectories of KcsA-E71A starting from the KWK configuration and membrane potential equal to +200 mV (orange line), and three non-collapsing trajectories of KcsA-WT starting from the KK configuration and membrane potential equal to +200 mV (light blue line).

Discussion

Potassium channels, and in particular KcsA, are ideal systems to validate the methods and force fields employed in MD simulations. The reason is twofold: the numerous 3D structure of different functional states available as starting models for computational studies, and the abundant experimental data at the single molecule level. Crucially, the timescale of ion conduction events

allows a direct comparison between the results of MD simulations and experimental measurements, facilitating a quantitative comparison between atomic trajectories and experimental observations. In this context, the MD simulations presented in this study have been used to assess the quality and reliability of two of the most common force fields employed in computer simulations of complex biological systems, AMBER and CHARMM.

The most striking difference between the two force fields concerns the stability of the open/conductive structure of the selectivity filter. In simulations using the AMBER force field, this open/conductive structure was stable on a microsecond timescale. In contrast, in simulations using the CHARMM force field, complete transitions between the open/conductive and the open-inactivated structure of the channel were observed on the same timescale. The fast collapse of the selectivity filter observed in simulations with the CHARMM force field is in apparent conflict with available experimental data on inactivation, as this process is orders of magnitude slower, taking place in the millisecond timescale [24]. Fast inactivation of wild-type KcsA in simulations with the CHARMM force field were also observed by Roux and collaborators [22]. They argued that opening of the intracellular gate is the rate-limiting step of inactivation rather than the collapse of the selectivity filter to justify these rapid collapsing events. However, we observed analogous collapsing events in simulations of KcsA-E71A. The starting model of KcsA-E71A was the high-resolution experimental structure of the channel in the open/conductive state, and as KcsA-E71A does not inactivate, inactivation events should not be observed in MD simulations, especially on a microsecond timescale. Fast inactivation events were reported also in MD simulations of the hERG K^+-channel using the CHARMM force field [25]. The simulations presented in this study discourage an interpretation of such structural changes of the selectivity filter as representative of early events involved in inactivation, as they are also observed in a non-inactivating channel. An alternative interpretation of these structural changes is that they represent rapid state transitions of a conductive selectivity filter. Rapid switching between alternative states of the selectivity filter was observed in MD simulations of other ion channels [26], and in the case of KcsA, these rapid movements are in agreement with experimental data that showed that the P-loop of the channel is a highly dynamic region [27]. While it is not possible to exclude this hypothesis, in our view, the most likely explanation for the fast collapse of the selectivity filter observed in MD simulations of KcsA with the CHARMM force field is a bias of this model toward the inactivated state of the selectivity filter. Indeed, in some of the MD trajectories, a complete transition from the conductive to the inactivated state of the selectivity filter was detected, while the opposite transition was never observed. Moreover, full recovery of binding sites S1-S4 was never achieved in any of the simulations where the selectivity filter deviated from the initial structure.

If these dynamics were representative of rapid structural changes of a conductive selectivity filter, transitions in both directions should be expected.

Most of the previous studies of conduction and selectivity in potassium channels were based on MD trajectories that rarely exceeded a few hundreds of nanoseconds in length which is possibly the upper limit of the temporal scale that these models were originally designed to sample reliably [28–31]. As deviations from the open/conductive structure emerges only in the microsecond timescale, the conclusions on conduction and selectivity reported earlier using shorter simulations can accurately describe the properties of the canonical open/conductive structure of the selectivity filter.

The second conclusion that can be drawn from the set of simulations performed in this study is that the estimated conductance was approximatively one order of magnitude lower than the experimental counterparts [19], both in simulations using the AMBER and CHARMM force fields. The atomic models used in the simulations only resembles partly the experimental set-up; the structure did not include the full intracellular domain of the channel, and the composition of the lipid bilayer is not identical. In addition, the simulation set-up also differs from the experimental one as a consequence of the periodic boundary conditions and the protocol used to impose the membrane potentials. The impact of these features on the estimated conductance values leaves room for future studies. In previous studies, the agreement between estimated and experimental conductance values was obtained only by adopting membrane potentials of 750 mV or above [13 25]. The risk of using high membrane potentials is to sample conduction strategies that are not representative of the normal channel functioning, or even to force the passage of ions across channel states that are actually occluded at physiological conditions. When membrane potentials are restricted to nearly physiological values, an underestimation of the channel conductance similar to the one observed here for KcsA was reported by Jensen et al. for the Kv1.2 channel using the CHARMM27 force field [13]. The fact that the channel conductance is underestimated by 1-2 orders of magnitude regardless of the force field or the ion channel model suggests that a similar shortcoming is responsible for this disagreement. The lack of polarization effects, which is a common characteristic of the classical force fields used in these studies, is an immediate candidate as the main source of error. Intensive efforts are underway to develop polarizable force fields for biomolecules simulations [32]. In the context of ion channels, the more accurate description of ions that is potentially offered by polarizable force fields when ions move between bulk water and protein functional groups [33], is a promising strategy to improve the agreement between experimental and computational values of channel conductance.

The shortcomings of MD simulations when it comes to a quantitative comparison with experimental data should not shadow the importance of the technique in the analysis of the structure-function relation in biological systems. In this respect, it is noteworthy to highlight the agreement in the results

obtained in simulations with the AMBER and CHARMM force fields. Firstly, the KK mechanism emerged as the dominant conduction strategy in both force fields under the conditions employed in the simulations, in agreement with previous results [17]. Furthermore, not only water molecules were excluded from participating in conduction events, but the presence of water in binding sites S2 or S3 impacted on the dynamics of the selectivity filter in simulations with both force fields. The effect of water molecules at S2 or S3 sites on the dynamics of the selectivity filter was critically different in simulations with the AMBER and the CHARMM force fields. In simulations with the AMBER force field, water molecules increased the likelihood of V76 flipping, while in the simulations with the CHARMM force field, water molecules accelerated the collapse of the selectivity filter. Nevertheless, in both cases, the structure of the selectivity filter remained closer to the open/conductive structure observed in crystallographic experiments in the absence of water molecules from the selectivity filter, which suggests a potential role of the water molecules at S2 or S3 sites for the inactivation process. In agreement with this hypothesis, the impact of water molecules in S2 and S3 was more severe in simulations of KcsA-WT than of KcsA-E71A, again regardless of the force field. The possible role of water molecules occupying S2 or S3 on inactivation might explain experimental data from KcsA channels mutated with amide-to-ester substitutions in residues G77 and Y78 [34]. Amide-to-ester substitutions at these residues decrease the likelihood of ions binding to S2, and the rate of inactivation. On the base of these experimental observations, it was concluded that an ion in S2 is necessary for inactivation, and consequently, that the collapsed state of the selectivity filter cannot be the inactivated state. However, amide-to-ester substitutions not only impact on ion binding, but also on water binding, as exemplified by the correlation between the presence of water and the flipping of V76. If water molecules in binding sites S2 and S3 are necessary for inactivation, as suggested by the simulations presented in this study, the lack of inactivation of KcsA channels with ester to amide substitutions in residues G77 and Y78 might results from the dehydration of the selectivity filter prompted by these mutations rather than by the lower ion occupancy of binding site S2.

Currently, MD simulations are widely used to interpret experimental data at atomic detail and to explore the structure-function relationship of complex biological systems. The data presented in this study clearly reveals some of the current shortcomings of MD simulations when it comes to a quantitative comparison with experimental data. Classical force fields were initially developed in the 1980s, when timescales accessible to MD simulations were very limited compared to today's standards. As longer timescales are steadily becoming the norm, the shortcomings of these force fields are becoming more apparent. Knowledge of these shortcomings and work to circumvent their limitations is crucial to further advance the field.

Methods

The channel models were based on the experimental structure of KcsA in the open/conductive state, Protein Data Bank entry 5VK6 [22]. The entire transmembrane domain of the channel, from residue Trp26 to residue Gln121, was considered in the models. The initial atomic coordinates of the systems were obtained with CHARMM-GUI [35]. The lipid membrane was a mixture of 1-palmitoyl-2-oleoyl-glycero-3-phosphocholine (POPC) and 1-palmitoyl-2-oleoyl-sn-glycero-3-phosphate (POPA), with a ratio of 3-POPC:1-POPA. The channel was inserted in the lipid membrane as defined in the Orientations of Proteins in Membranes (OPM) database [36]. The systems were solvated using TIP3P water molecules [37] (~15.000 molecules) and ions to reach a 200 mM of KCl. Potassium ions were manually placed at binding sites S0, S2 and S4. For KWK simulations, water molecules were also manually placed in S1 and S3 binding sites. The crystallographic water molecules at the back of the selectivity filter, close to residues Ala17 and Gly79, were preserved in the KcsA-E71A model. For the definition of KcsA-WT, the alanine residue at position 71 was manually modified to glutamate. For simulations with the CHARMM force field, the latest version of CHARMM36 was used [38]. When explicitly indicated, the Lennard-Jones parameters of K^+ were modified by NBFIX terms [39], or alternatively the ion parameters by Joung and Cheatham [23] were adopted. van der Waals interactions were smoothly truncated between 10 and 12 Å. For simulations with the AMBER force field, the ff14sb version was used [40], in combination with ion parameters by Joung and Cheatham [23] for the TIP3P water model. van der Waals interactions were truncated at 9 Å. Standard AMBER scaling of 1-4 interactions was applied. The same equilibration protocol was used for simulations with both force fields, consisting of 10.000 of energy minimization, followed by 10 ns in the NPT ensemble with timestep equal to 1 fs and 60 ns in the NPT ensemble with timestep equal to 2 fs. In the course of the equilibration protocol, restraints on protein and lipid atoms were gradually reduced to zero. Long-range electrostatic interactions were calculated with the Particle Mesh Ewald method using a grid spacing of 1.0 Å [41]. The SETTLE algorithm was used to restrain bonds with the hydrogen atom [42]. The temperature was controlled at 310 K by coupling to a Langevin thermostat with a damping coefficient of 1 ps^{-1}. A pressure of 1 atm was maintained by coupling the system to a Nose−Hoover Langevin piston, with a damping constant of 25 ps and a period of 50 ps [43]. The presence of membrane potentials was mimicked by applying a constant electric field acting in the direction perpendicular to the lipid membrane. The simulations with external electric field were performed in the NVT ensemble. All the simulations were rendered using NAMD2.11 [44].

ACKNOWLEDGEMENTS. We acknowledge PRACE for awarding access to computational resources in CSCS, the Swiss National Supercomputing Service, in the 17th Project Access Call.

SUPPORTING INFORMATION. List of MD simulations (Table S1). Ion trajectories (Figures S1,3,5-7,10,11,13). Dihedral angles of the selectivity filter (Figures S2,4). Diameter of the selectivity filter (Figures S8,9,12). This information is available free of charge via the Internet at http://pubs.acs.org.

References

(1) Hodgkin, A. L.; Huxley, A. F. A Quantitative Description of Membrane Current and Its Application to Conduction and Excitation in Nerve. *J. Physiol.* **1952**, *117* (4), 500–544.

(2) Doyle, D. A.; Cabral, J. M.; Pfuetzner, R. A.; Kuo, A.; Gulbis, J. M.; Cohen, S. L.; Chait, B. T.; MacKinnon, R. The Structure of the Potassium Channel: Molecular Basis of K+ Conduction and Selectivity. *Science (80-.).* **1998**, *280* (5360), 69–77.

(3) Chakrapani, S.; Cordero-Morales, J. F.; Perozo, E. A Quantitative Description of KcsA Gating I: Macroscopic Currents. *J. Gen. Physiol.* **2007**, *130* (5), 465–478.

(4) Cordero-Morales, J. F.; Cuello, L. G.; Zhao, Y.; Jogini, V.; Cortes, D. M.; Roux, B.; Perozo, E. Molecular Determinants of Gating at the Potassium-Channel Selectivity Filter. *Nat. Struct. Mol. Biol.* **2006**, *13* (4), 311–318.

(5) Cuello, L. G.; Jogini, V.; Cortes, D. M.; Perozo, E. Structural Mechanism of C-Type Inactivation in K+ Channels. *Nature* **2010**, *466* (7303), 203–208.

(6) Cordero-Morales, J. F.; Jogini, V.; Lewis, A.; Vásquez, V.; Cortes, D. M.; Roux, B.; Perozo, E. Molecular Driving Forces Determining Potassium Channel Slow Inactivation. *Nat. Struct. Mol. Biol.* **2007**, *14* (11), 1062–1069.

(7) Ostmeyer, J.; Chakrapani, S.; Pan, A. C.; Perozo, E.; Roux, B. Recovery from Slow Inactivation in K+ Channels Is Controlled by Water Molecules. *Nature* **2013**, *501* (7465), 121–124.

(8) Aqvist, J.; Luzhkov, V. Ion Permeation Mechanism of the Potassium Channel. *Nature* **2000**, *404* (6780), 881–884.

(9) Domene, C.; Sansom, M. S. P. Potassium Channel, Ions, and Water: Simulation Studies Based on the High Resolution X-Ray Structure of KcsA. *Biophys. J.* **2003**, *85* (5), 2787–2800.

(10) Chung, S. H.; Allen, T. W.; Kuyucak, S. Conducting-State Properties of the KcsA Potassium Channel from Molecular and Brownian Dynamics Simulations. *Biophys. J.* **2002**, *82* (2),

628–645.

(11) Bernèche, S.; Roux, B. Energetics of Ion Conduction through the K+ Channel. *Nature* **2001**, *414* (6859), 73–77.

(12) Bernsteiner, H.; Zangerl-Plessl, E. M.; Chen, X.; Stary-Weinzinger, A. Conduction through a Narrow Inward-Rectifier K+ Channel Pore. *J. Gen. Physiol.* **2019**, *151* (10), 1231–1246.

(13) Jensen, M. Ø.; Jogini, V.; Eastwood, M. P.; Shaw, D. E. Atomic-Level Simulation of Current–Voltage Relationships in Single-File Ion Channels. *J. Gen. Physiol.* **2013**, *141* (5), 619–632.

(14) Furini, S.; Domene, C. Atypical Mechanism of Conduction in Potassium Channels. *Proc. Natl. Acad. Sci.* **2009**, *106* (38), 16074–16077.

(15) Köpfer, D. A.; Song, C.; Gruene, T.; Sheldrick, G. M.; Zachariae, U.; De Groot, B. L. Ion Permeation in K+ Channels Occurs by Direct Coulomb Knock-On. *Science (80-.).* **2014**, *346* (6207), 352–355.

(16) Morais-Cabral, J. H. H.; Zhou, Y.; MacKinnon, R. Energetic Optimization of Ion Conduction Rate by the K+ Selectivity Filter. *Nature* **2001**, *414* (6859), 37–40.

(17) Kopec, W.; Köpfer, D. A.; Vickery, O. N.; Bondarenko, A. S.; Jansen, T. L. C.; de Groot, B. L.; Zachariae, U. Direct Knock-on of Desolvated Ions Governs Strict Ion Selectivity in K+ Channels. *Nat. Chem.* **2018**, *10* (8), 813–820.

(18) Kratochvil, H. T.; Carr, J. K.; Matulef, K.; Annen, A. W.; Li, H.; Maj, M.; Ostmeyer, J.; Serrano, A. L.; Raghuraman, H.; Moran, S. D.; Skinner, J. L.; Perozo, E.; Roux, B.; Valiyaveetil, F. I.; Zanni, M. T. Instantaneous Ion Configurations in the K+ion Channel Selectivity Filter Revealed by 2D IR Spectroscopy. *Science (80-.).* **2016**, *353* (6303), 1040–1044.

(19) Cuello, L. G.; Cortes, D. M.; Perozo, E. The Gating Cycle of a K+ Channel at Atomic Resolution. *Elife* **2017**, *6*, 1–17.

(20) Zhou, Y.; Morais-Cabral, J. H.; Kaufman, A.; Mackinnon, R. Chemistry of Ion Coordination and Hydration Revealed by a K+ Channel-Fab Complex at 2.0 Å Resolution. *Nature* **2001**, *414* (6859), 43–48.

(21) Bernèche, S.; Roux, B. A Gate in the Selectivity Filter of Potassium Channels. *Structure* **2005**, *13* (4), 591–600.

(22) Li, J.; Ostmeyer, J.; Cuello, L. G.; Perozo, E.; Roux, B. Rapid Constriction of the Selectivity Filter Underlies C-Type Inactivation in the KcsA Potassium Channel. *J. Gen. Physiol.* **2018**, *215* (10), 1408–1420.

(23) Joung, I. S.; Cheatham, T. E. Determination of Alkali and Halide Monovalent Ion Parameters

for Use in Explicitly Solvated Biomolecular Simulations. *J. Phys. Chem. B* **2008**, *112* (30), 9020–9041.

(24) Chakrapani, S.; Cordero-Morales, J. F.; Perozo, E. A Quantitative Description of KcsA Gating II: Single-Channel Currents. *J. Gen. Physiol.* **2007**, *130* (5), 479–496.

(25) Miranda, W. E.; DeMarco, K. R.; Guo, J.; Duff, H. J.; Vorobyov, I.; Clancy, C. E.; Noskov, S. Y. Selectivity Filter Modalities and Rapid Inactivation of the HERG1 Channel. *Proc. Natl. Acad. Sci. U. S. A.* **2020**, *117* (6), 2795–2804.

(26) Furini, S.; Domene, C. Ion-Triggered Selectivity in Bacterial Sodium Channels. *Proc Natl Acad Sci USA* **2018**, *22* (21), 5450–5455.

(27) Jekhmane, S.; Medeiros-Silva, J.; Li, J.; Kümmerer, F.; Müller-Hermes, C.; Baldus, M.; Roux, B.; Weingarth, M. Shifts in the Selectivity Filter Dynamics Cause Modal Gating in K + Channels. *Nat. Commun.* **2019**, *10* (1), 1–12.

(28) Furini, S.; Domene, C. K+ and Na+ Conduction in Selective and Nonselective Ion Channels Via Molecular Dynamics Simulations. *Biophys. J.* **2013**, *105* (8), 1737–1745.

(29) Flood, E.; Boiteux, C.; Lev, B.; Vorobyov, I.; Allen, T. W. Atomistic Simulations of Membrane Ion Channel Conduction, Gating, and Modulation. *Chem. Rev.* **2019**, *119* (13), 7737–7832.

(30) Maffeo, C.; Bhattacharya, S.; Yoo, J.; Wells, D.; Aksimentiev, A. Modeling and Simulation of Ion Channels. *Chem. Rev.* **2012**, *112* (12), 6250–6284.

(31) Furini, S.; Domene, C. Computational Studies of Transport in Ion Channels Using Metadynamics. *Biochim. Biophys. Acta - Biomembr.* **2016**, *1858* (7), 1733–1740.

(32) Lemkul, J. A.; Huang, J.; Roux, B.; Mackerell, A. D. An Empirical Polarizable Force Field Based on the Classical Drude Oscillator Model: Development History and Recent Applications. *Chem. Rev.* **2016**, *116* (9), 4983–5013.

(33) Wineman-Fisher, V.; Al-Hamdani, Y.; Addou, I.; Tkatchenko, A.; Varma, S. Ion-Hydroxyl Interactions: From High-Level Quantum Benchmarks to Transferable Polarizable Force Fields. *J. Chem. Theory Comput.* **2019**, *15* (4), 2444–2453.

(34) Matulef, K.; Annen, A. W.; Nix, J. C.; Valiyaveetil, F. I. Individual Ion Binding Sites in the K+ Channel Play Distinct Roles in C-Type Inactivation and in Recovery from Inactivation. *Structure* **2016**, *24* (5), 750–761.

(35) Jo, S.; Kim, T.; Iyer, V. G.; Im, W. CHARMM-GUI: A Web-Based Graphical User Interface for CHARMM. *J. Comput. Chem.* **2008**, *29* (11), 1859–1865.

(36) Lomize, M. A.; Pogozheva, I. D.; Joo, H.; Mosberg, H. I.; Lomize, A. L. OPM Database and PPM Web Server : Resources for Positioning of Proteins in Membranes. **2012**, *40*

(September 2011), 370–376.

(37) Jorgensen, W. L.; Chandrasekhar, J.; Madura, J. D.; Impey, R. W.; Klein, M. L. Comparison of Simple Potential Functions for Simulating Liquid Water. *J. Chem. Phys.* **1983**, *79* (2), 926–935.

(38) Huang, J.; Rauscher, S.; Nawrocki, G.; Ran, T.; Feig, M.; de Groot, B. L.; Grubmüller, H.; MacKerell Jr, A. D. CHARMM36m: An Improved Force Field for Folded and Intrinsically Disordered Proteins. *Nat. Methods* **2016**, *14*, 71.

(39) Noskov, S. Y.; Bernéche, S.; Roux, B. Control of Ion Selectivity in Potassium Channels by Electrostatic and Dynamic Properties of Carbonyl Ligands. *Nature* **2004**, *431* (7010), 830–834.

(40) Maier, J. A.; Martinez, C.; Kasavajhala, K.; Wickstrom, L.; Hauser, K. E.; Simmerling, C. Ff14SB: Improving the Accuracy of Protein Side Chain and Backbone Parameters from Ff99SB. *J. Chem. Theory Comput.* **2015**, *11* (8), 3696–3713.

(41) Essmann, U.; Perera, L.; Berkowitz, M. L.; Darden, T.; Lee, H.; Pedersen, L. G. A Smooth Particle Mesh Ewald Method. *J. Chem. Phys.* **1995**, *103* (19), 8577–8593.

(42) Tuckerman, M.; Berne, B. J.; Martyna, G. J. Reversible Multiple Time Scale Molecular Dynamics. *J. Chem. Phys.* **1992**, *97* (3), 1990–2001.

(43) Feller, S. E.; Zhang, Y.; Pastor, R. W.; Brooks, B. R. Constant Pressure Molecular Dynamics Simulation: The Langevin Piston Method. *J. Chem. Phys.* **1995**, *103* (11), 4613–4621.

(44) Phillips, J. C.; Braun, R.; Wang, W.; Gumbart, J.; Tajkhorshid, E.; Villa, E.; Chipot, C.; Skeel, R. D.; Kalé, L.; Schulten, K. Scalable Molecular Dynamics with NAMD. *J. Comput. Chem.* **2005**, *26* (16), 1781–1802.

(a)

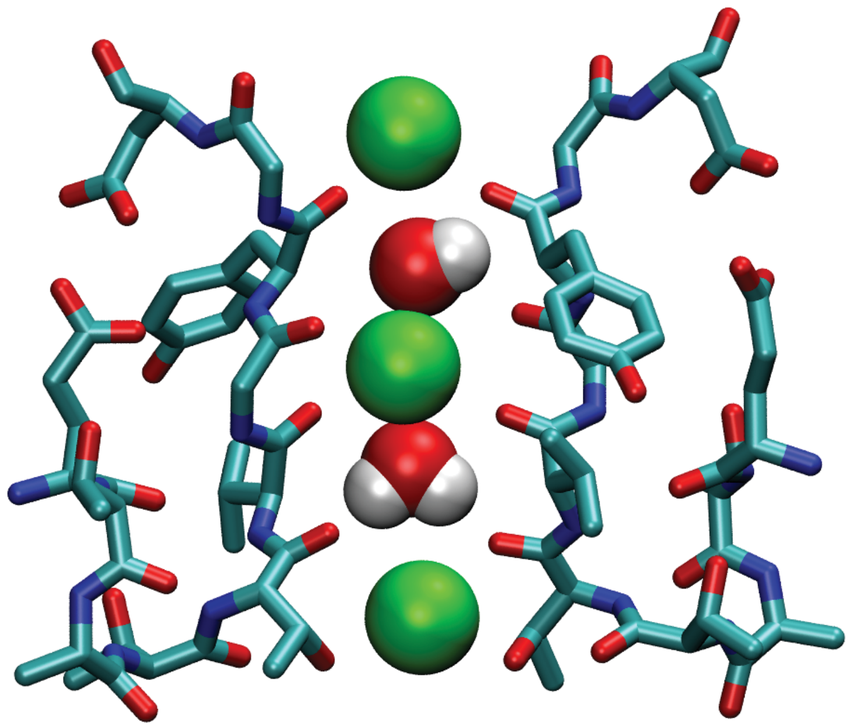

(b)

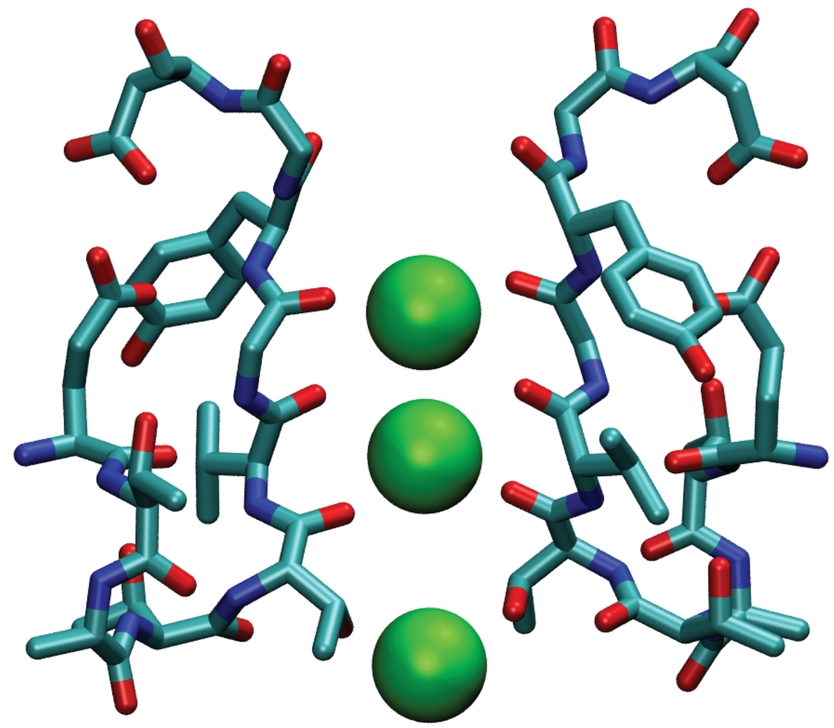

(c)

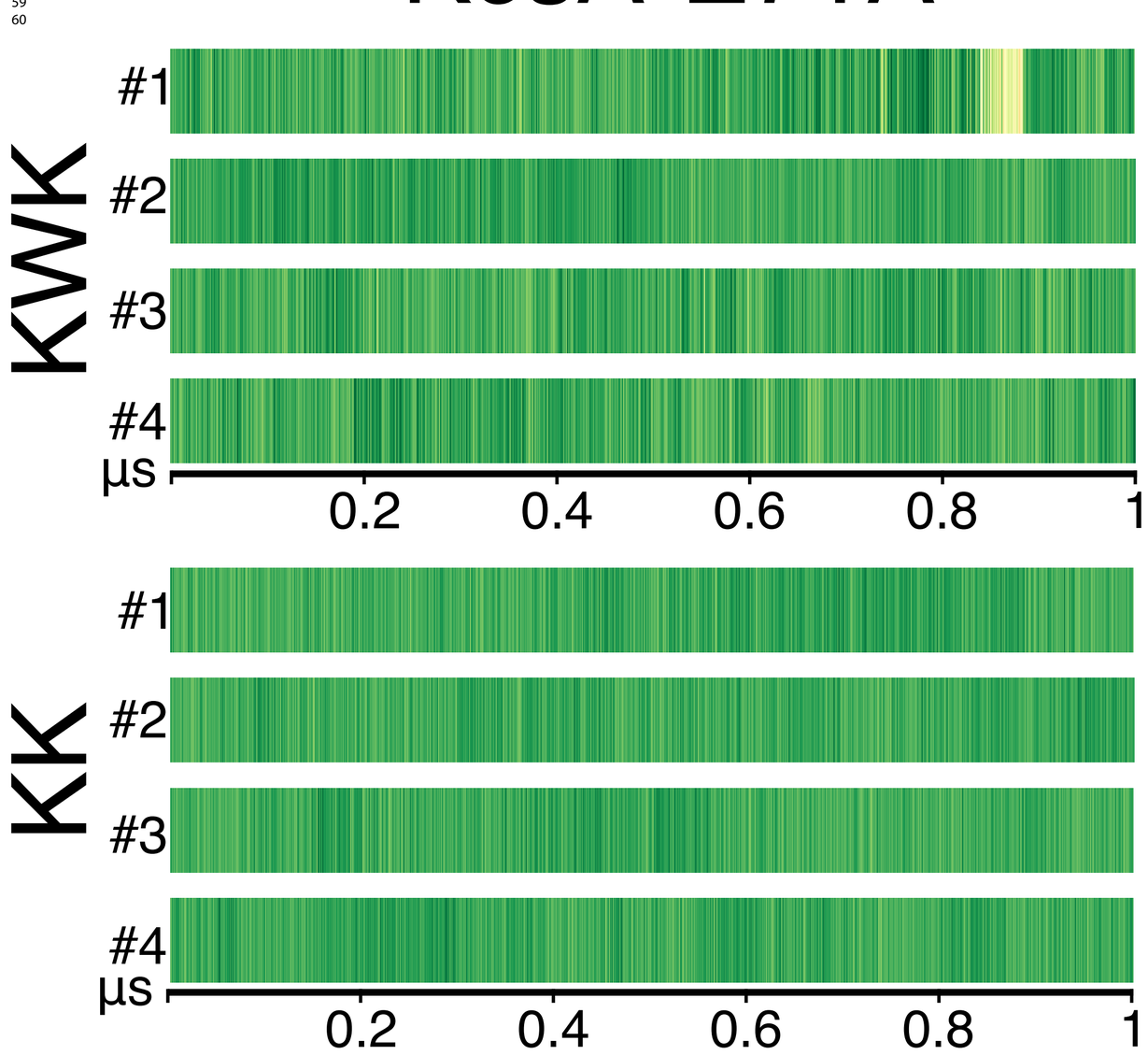

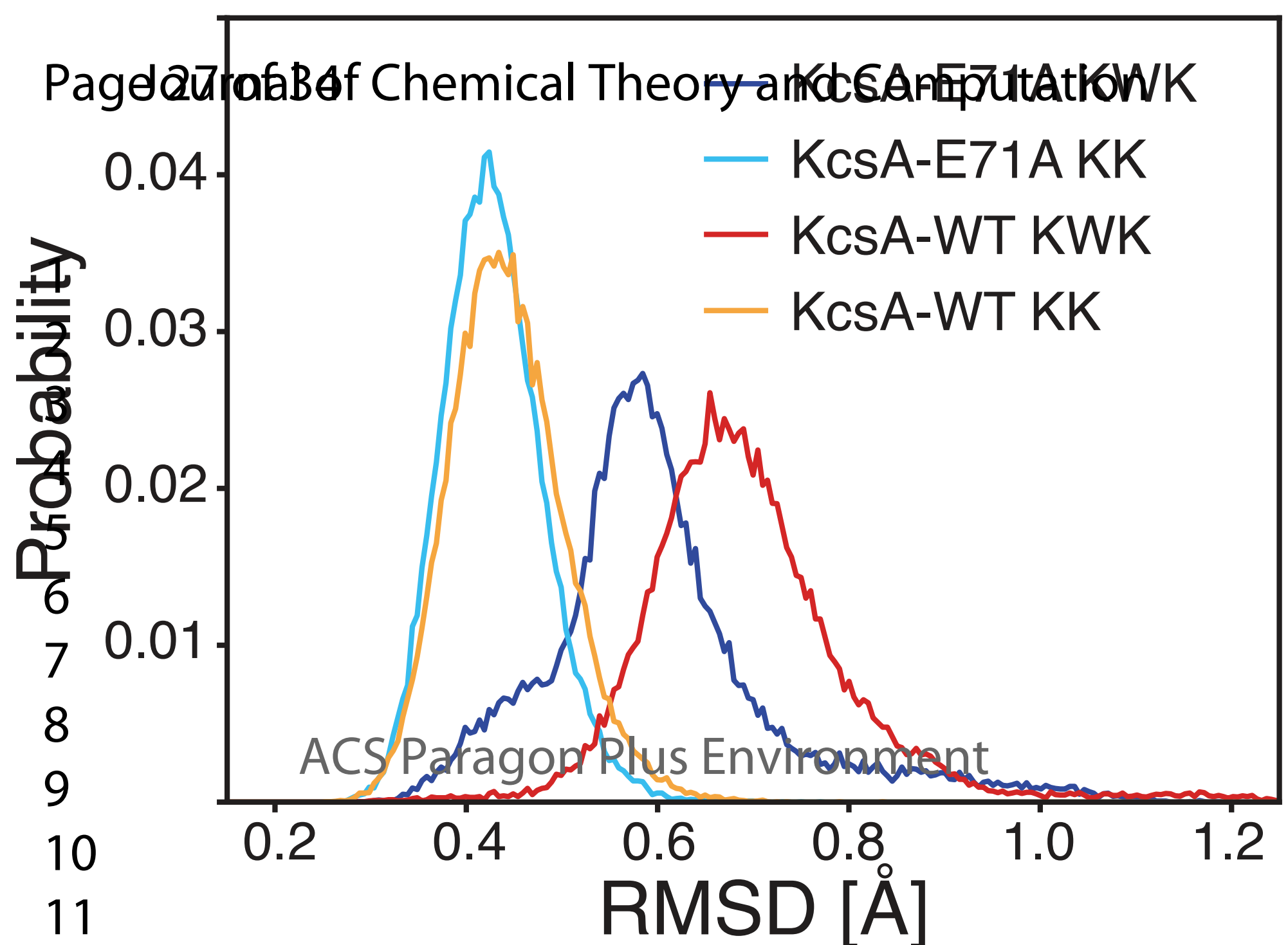
KcsA-E71A KWK
KcsA-E71A KK
KcsA-WT KWK
KcsA-WT KK
Probability
0.04
0.03
0.02
0.01
0.2
0.4
0.6
0.8
1.0
1.2
RMSD [Å]
ACS Paragon Plus Environment

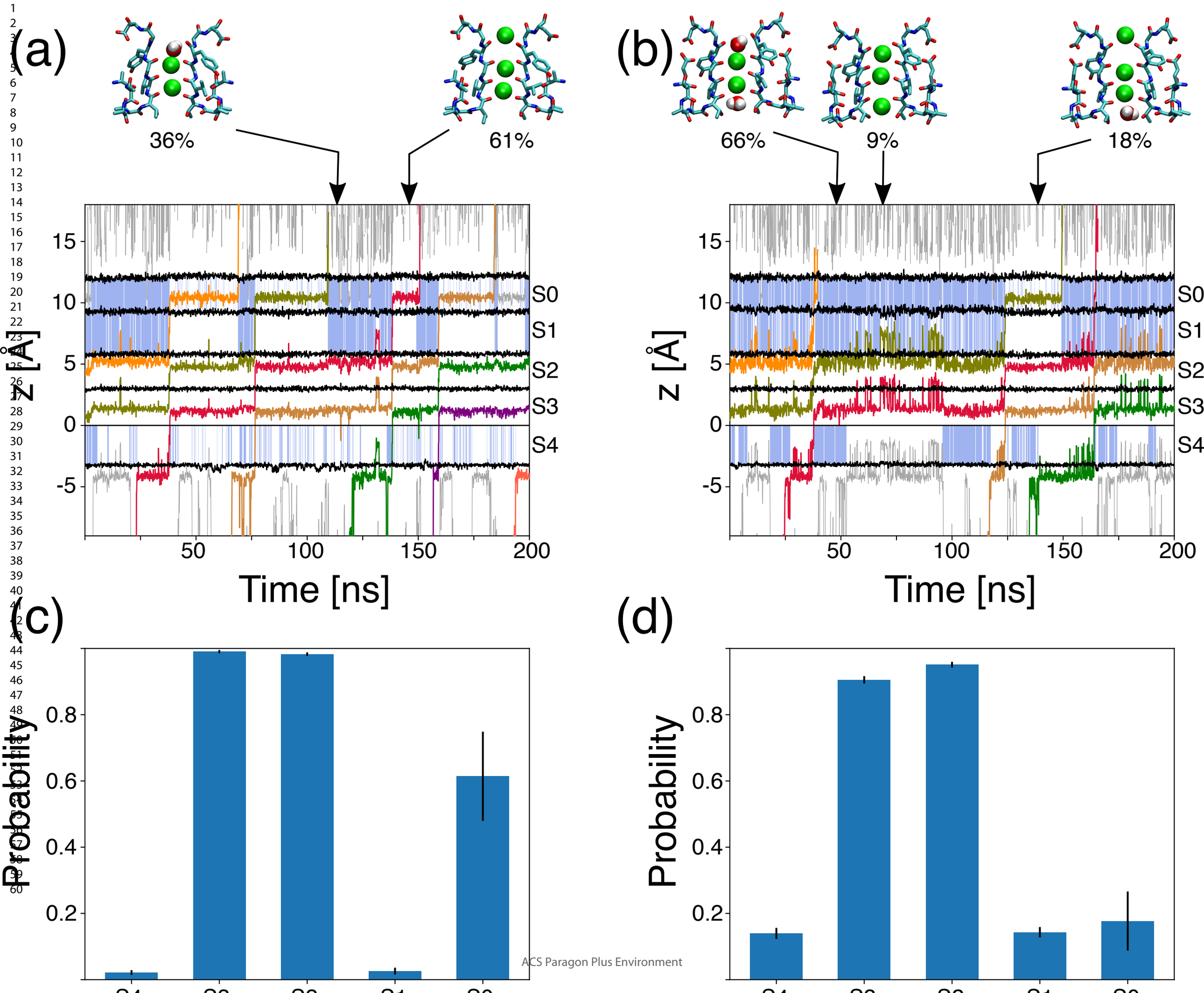

(a)

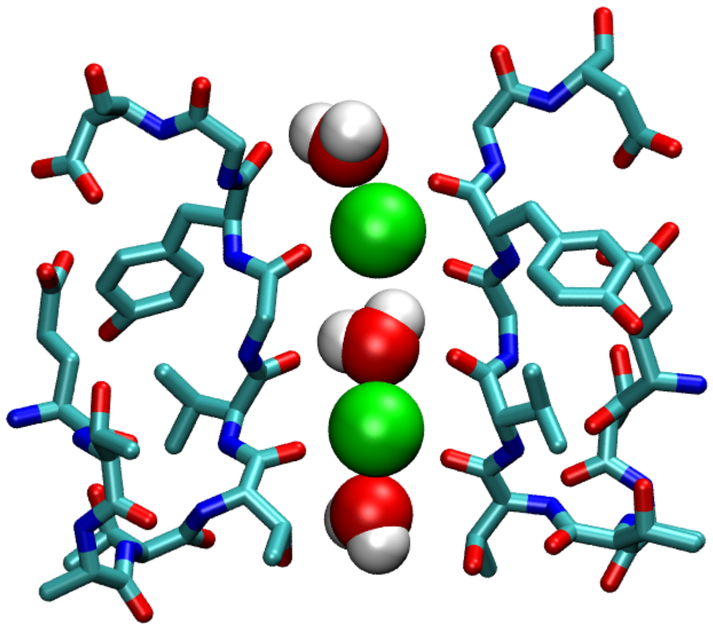

(b)

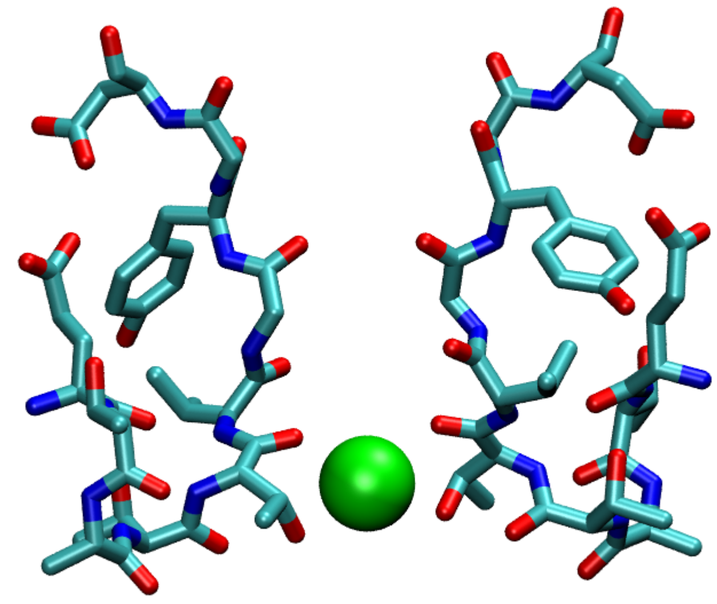

(c)

KcsA-E71A

KcsA-WT

KWK

KK

#1
#2
#3
#4
μs

0.2
0.4
0.6
0.8
1

4
5
6
7
8
9

Selectivity Filter diameter [Å]

(a)

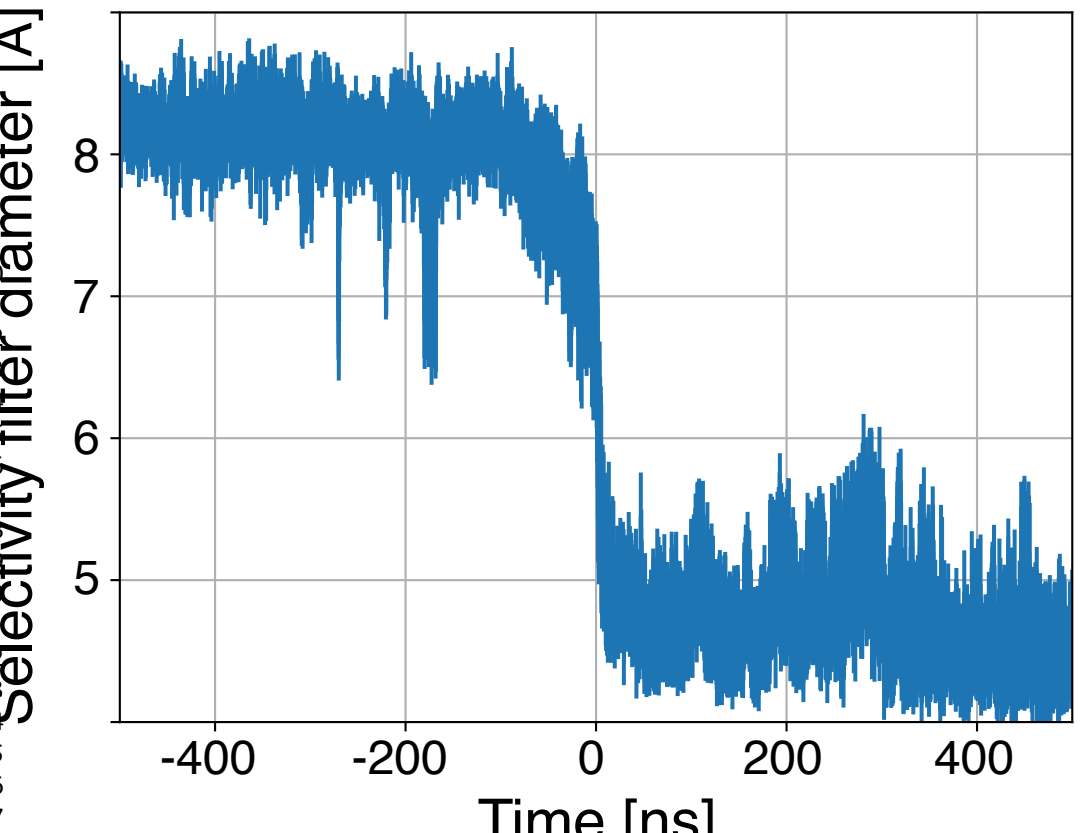

(b)

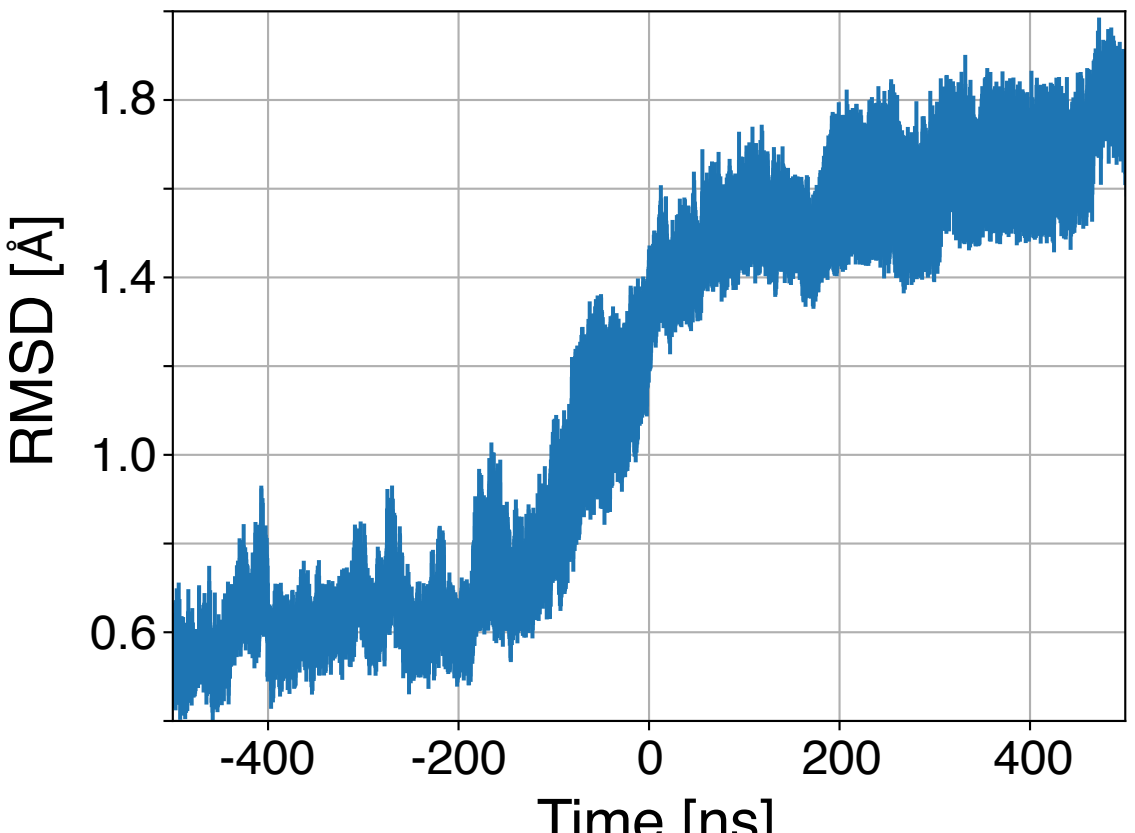

(c)

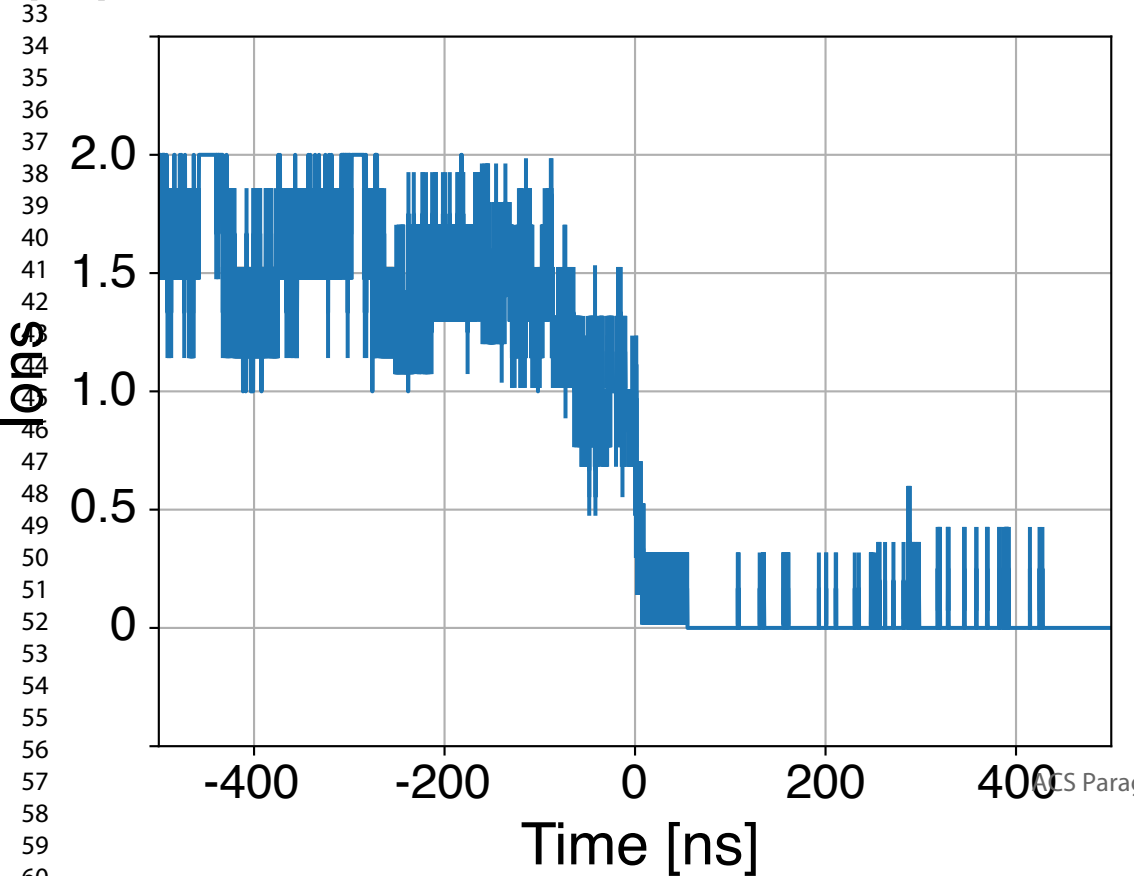

(d)

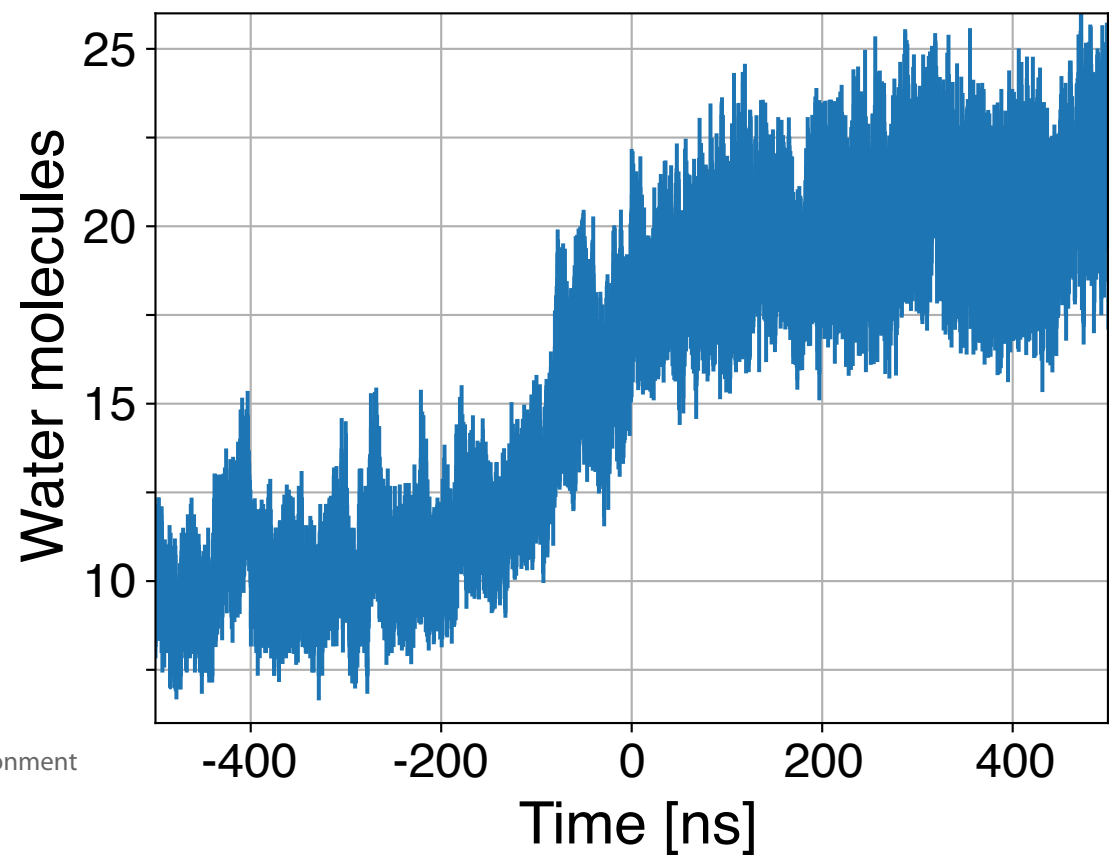

(a)

KcsA-E71A

+100 mV

+200 mV

KWK

#1
#2
#3
#4
μs

0.2 0.4 0.6 0.8 1

(b)

KcsA-WT

+100 mV

+200 mV

KK

#1
#2
#3
#4
μs

0.2 0.4 0.6 0.8 1

4 5 6 7 8 9

Selectivity Filter diameter [A]

KcsA-E71A

KcsA-WT

(a)

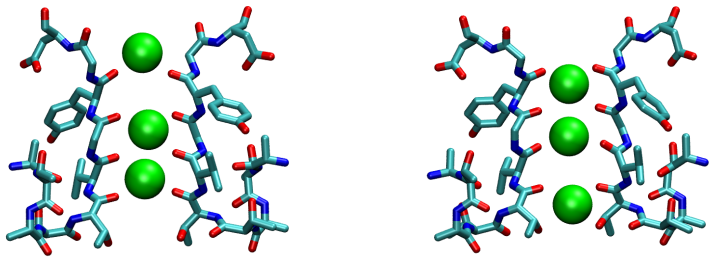

58%

22%

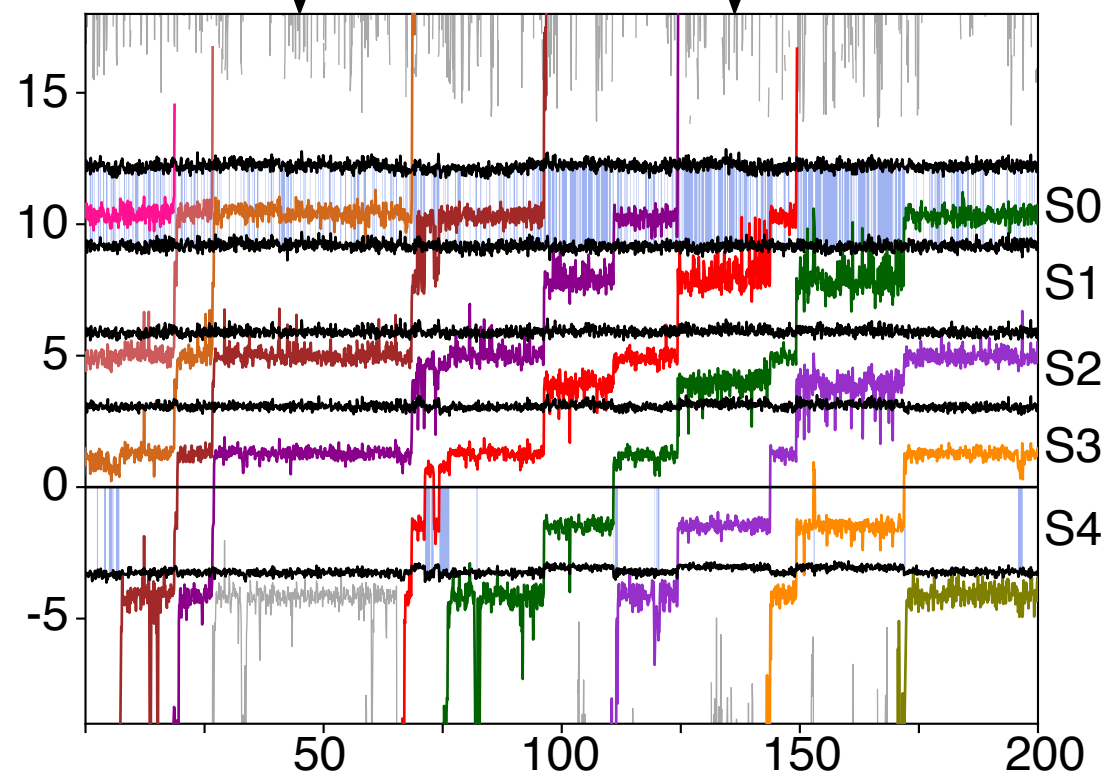

(b)

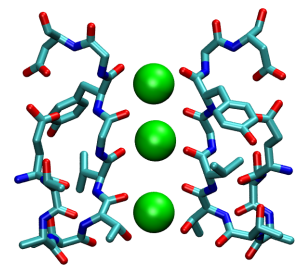

97%

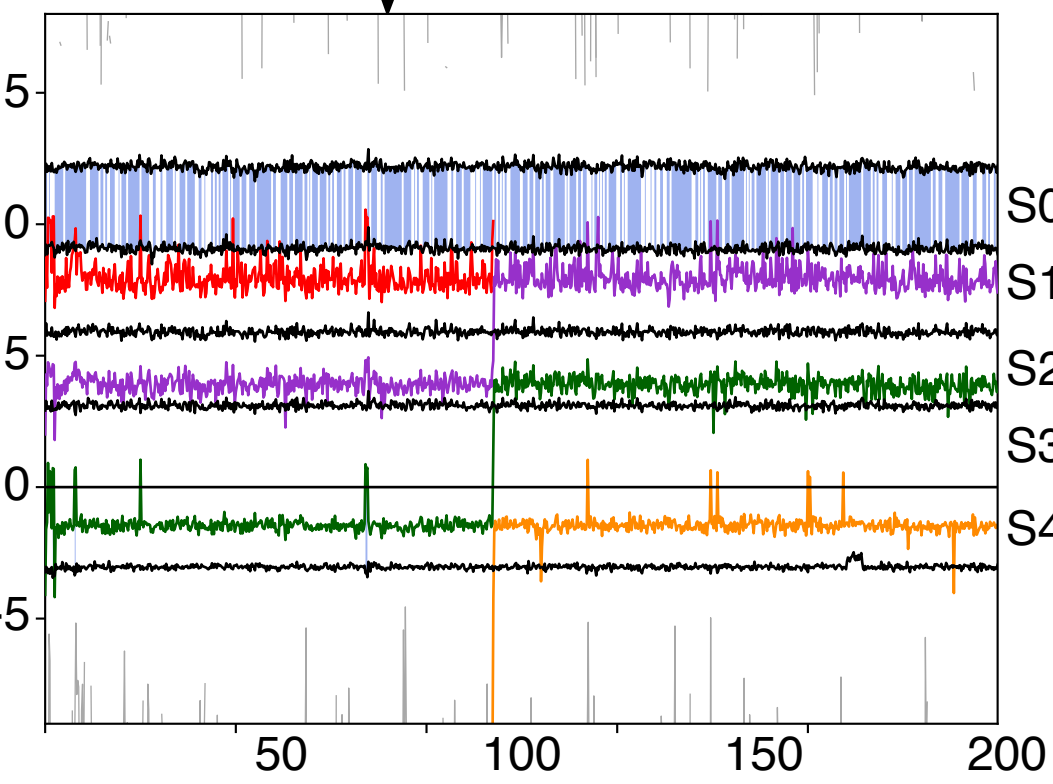

(c)

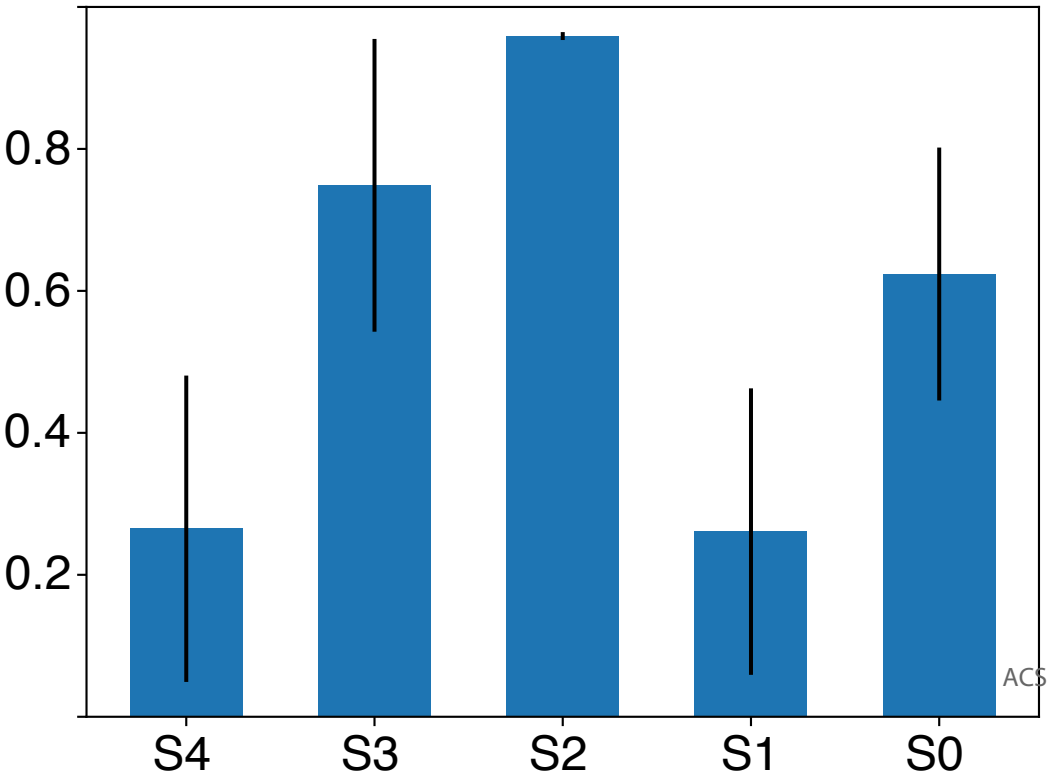

(d)

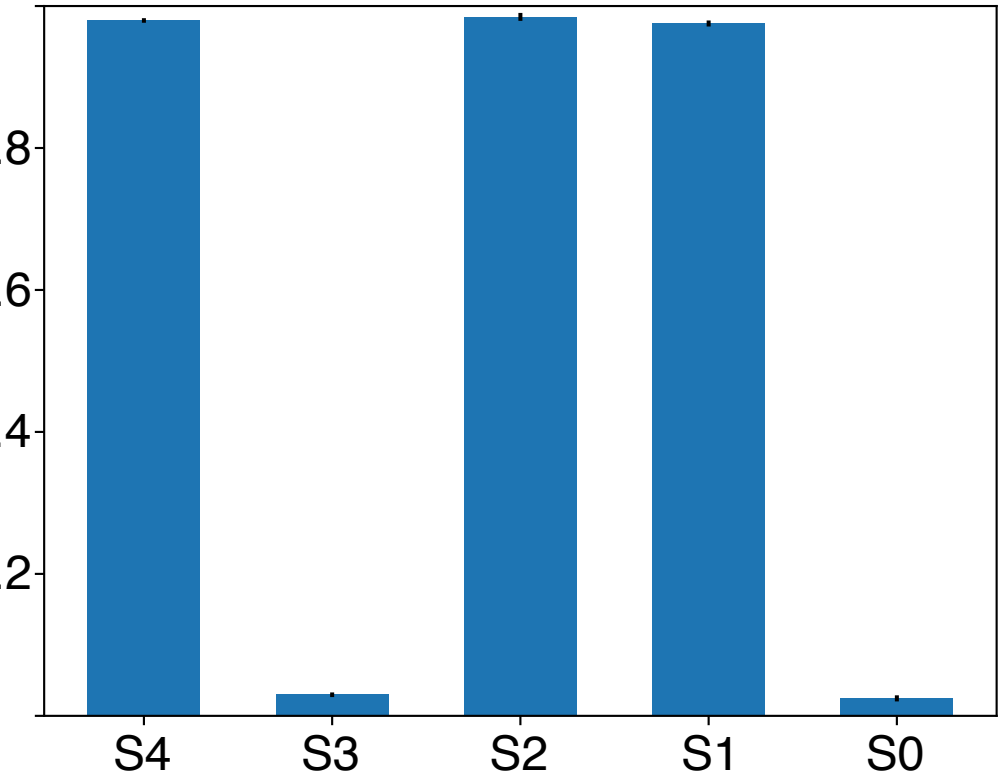

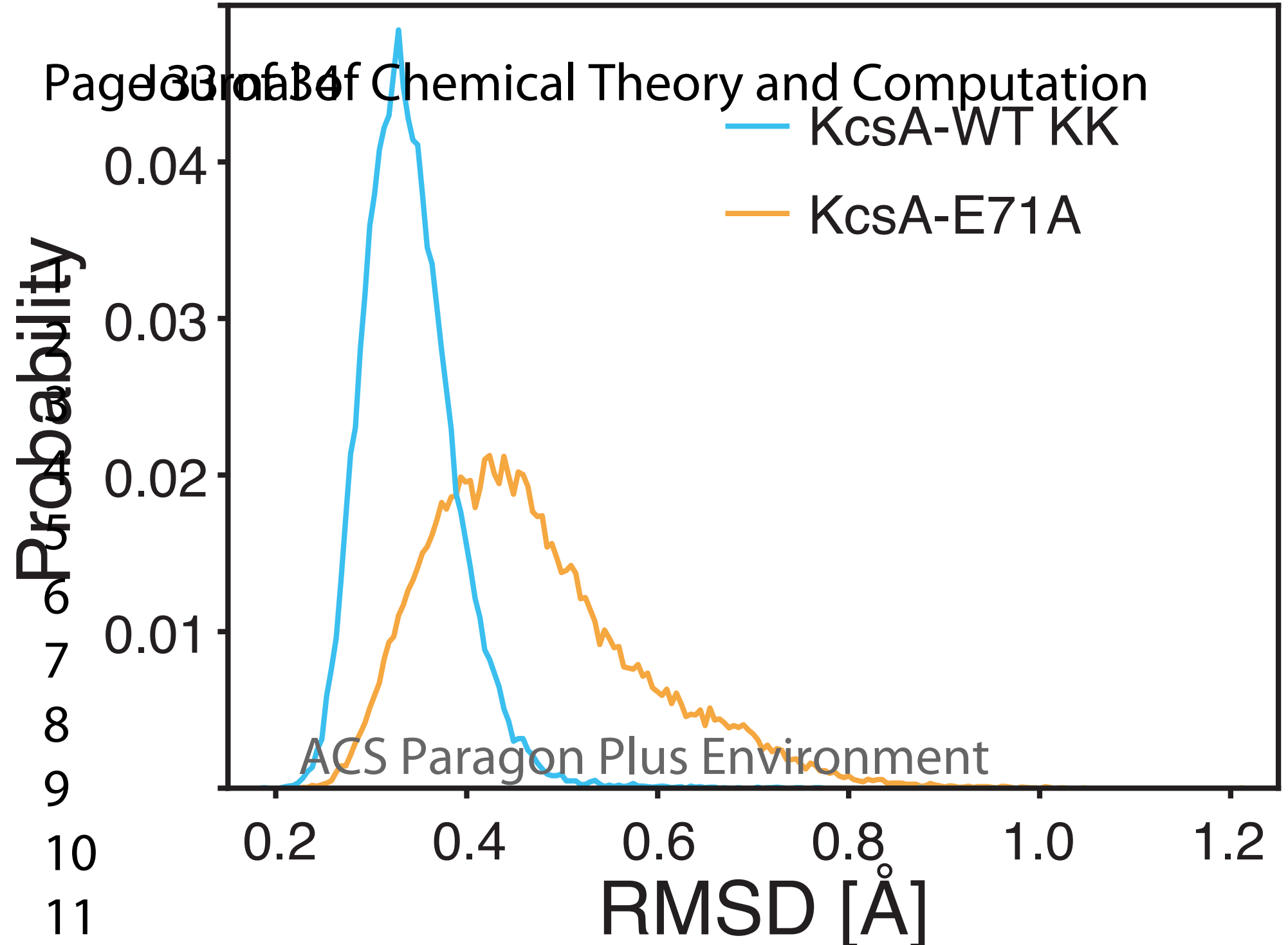
KcsA-WT KK
KcsA-E71A
Probability
0.04
0.03
0.02
0.01
0.2
0.4
0.6
0.8
1.0
1.2
RMSD [Å]
ACS Paragon Plus Environment